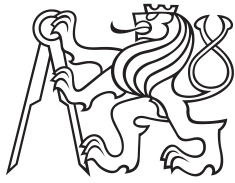**Bachelor's Thesis**

Czech Technical University in Prague

F3
Faculty of Electrical Engineering
Department of Control Engineering

Over-actuated vehicles energy efficiency evaluation

Kateřina Hobzová

BACHELOR'S THESIS ASSIGNMENT

I. Personal and study details

Student's name: **Hobzová Kateřina**   Personal ID number: **491823**

Faculty / Institute: **Faculty of Electrical Engineering**

Department / Institute: **Department of Control Engineering**

Study program: **Cybernetics and Robotics**

II. Bachelor's thesis details

Bachelor's thesis title in English:

Over-actuated vehicles energy efficiency evaluation

Bachelor's thesis title in Czech:

Vyhodnocení energetické účinnosti vozidel s více stupni volnosti

Guidelines:

The goal of this thesis is to develop algorithms for energy efficiency evaluation of vehicles with more degree of freedom.
The development of vehicles with electric powertrain and corner modules opens new possibilities for path tracking strategies.
The outcome of this thesis shall propose algorithms of energy efficiency evaluation of vehicle maneuvers.
1. Get familiar with vehicle dynamic mathematical models and implement suitable one.
2. Get familiar with path tracking algorithms.
3. Develop and implement methodology for energy evaluation of over-actuated vehicles.
4. Developed algorithms testing.

Bibliography / sources:

[1] Dieter Schramm, Manfred Hiller, Roberto Bardini – Vehicle Dynamics – Duisburg 2014
[2] Hans B. Pacejka - Tire and Vehicle Dynamics – The Netherlands 2012
[3] Robert Bosch GmbH - Bosch automotive handbook - Plochingen, Germany : Robet Bosch GmbH ; Cambridge, Mass.
: Bentley Publishers
[4] Rajamani R. (2012) Mean Value Modeling of SI and Diesel Engines. In: Vehicle Dynamics and Control. Mechanical
Engineering Series. Springer, Boston, MA. https://doi.org/10.1007/978-1-4614-1433-9_9

Name and workplace of bachelor's thesis supervisor:

doc. Ing. Tomáš Haniš, Ph.D.   Department of Control Engineering FEE

Name and workplace of second bachelor's thesis supervisor or consultant:

Date of bachelor's thesis assignment: **18.08.2023**   Deadline for bachelor thesis submission: **09.01.2024**

Assignment valid until:
by the end of summer semester 2023/2024

_____   _____   _____
doc. Ing. Tomáš Haniš, Ph.D.   prof. Ing. Michael Šebek, DrSc.   prof. Mgr. Petr Páta, Ph.D.
Supervisor's signature   Head of department's signature   Dean's signature

III. Assignment receipt

The student acknowledges that the bachelor's thesis is an individual work. The student must produce her thesis without the assistance of others,
with the exception of provided consultations. Within the bachelor's thesis, the author must state the names of consultants and include a list of references.

.
_____   _____
Date of assignment receipt   Student's signature

iv

Acknowledgements

First of all, I would like to express my gratitude to my supervisor, doc. Ing. Tomáš Haniš, Ph.D., for his expert guidance and patience while working on this thesis. Secondly, I would like to thank all my former tutors at the Faculty of Electrical Engineering of Czech Technical University in Prague. I am grateful for having the opportunity to study at such a prestigious university and for the resources this university provides for students. Finally, a very special thanks belongs to my family and my best friends without whose support and encouragement, my studies would not have been the same.

Declaration

I, Kateřina Hobzová, that this thesis titled, "Over-actuated vehicles energy efficiency evaluation" and the work presented in it are my own. I confirm that where I have consulted the published work of others, this is always clearly attributed and where I have quoted from the work of others, the source is always given in bibliography. With the exception of such quotations, this thesis is entirely my own work. I further confirm that I have acknowledged all main sources of help and where the thesis is based on work done by myself jointly with others, I have made clear exactly what was done by others and what I have contributed my- self.

In Prague, 6. January 2024

_____

Abstract

The objective of this thesis is to evaluate energy efficiency in over-actuated vehicles, focusing on dynamic control and high-level path-tracking algorithms. For the purposes of the thesis a twin-track model with a kinematic reference model, integrating high-level and low-level control systems was designed. Experiments examine energy efficiency across various scenarios with usage of control systems. The efficiency then evaluated in comparison to vehicle without any control system. The finding provide insight into optimizing of energy efficiency in electric vehicles.

Keywords: Energy efficiency evaluation, vehicle traction control, path tracking, torque vectoring, four-wheel-independent-drive, over-actuated vehicle, control system design, vehicle dynamics control, twin-track vehicle model

Supervisor: doc. Ing. Tomáš Haniš, Ph.D
Karlovo náměstí 13-E,Prague 2

Abstrakt

Cílem této práce je vyhodnotit energetickou účinnost vozidel s více stupni volnosti se zaměřením na dynamické řízení a algoritmy sledování trati. Pro účely této práce byl navržen model dvoustopý model vozidla s kinematickým referenčním modelem, který začleňuje vysokoúrovňový a nízkoúrovňový řídicí systém. Experimenty zkoumají energetickou účinnost pro různé scénáře s využitím řídicích systémů. Účinnost se pak vyhodnocuje ve srovnání s vozidlem bez jakéhokoli řídicího systému. Zjištění poskytují vhled do optimalizace energetické účinnosti elektrických vozidel.

Klíčová slova: Vyhodnocení energetické účinnosti,kontrola trakce vozidla, vedení po trati, asymetrické rozdělení trakčního momentu, vozidlo s nezávislým pohonem všech kol, vozidlo s více stupni volnosti, návrh řídicího systému, řízení dynamiky vozidla, dvoustopý model vozidla

Překlad názvu: Vyhodnocení energetické účinnosti vozidel s více stupni volnosti

Contents

Figures

ix

Tables

Chapter 1

Introduction

This thesis aims to evaluate the energy efficiency of a vehicle model and analyze driving resistance on different levels of the vehicle for different driving scenarios based on basic heuristics. Furthermore, we want to quantify the isolable or controllable factors so that they can be further controlled. For those purposes, an architecture was implemented using the twin-track model as the primary model and a kinematic model as a reference model, a high-level control system, and a low-level control system.

1.1 Motivation

Energy (from Greek $\epsilon\nu\epsilon\rho\gamma\iota\alpha$ (enérgeia) 'activity') is in physics capacity for doing or ability to do work. Everything around us works based on exchanging and conserving energy. As the law of conservation of energy states - energy can be neither created nor destroyed. People have been for civilizations committed to discovering different ways to transform different forms of energies between each other and how to use them to make their lives easier and more comfortable.

In the Stone Age, meals were cooked on bonfires, and fire torches were used as a source of light during the night. People would use animals, water, and wind as a source of power for different tools and devices such as hammer mills, plows, windmills, and tonnes of others. "During the 18th century, a good horse was considered to be equivalent to 10 men, or at least 700 W and the best horses would eventually surpass power equivalent to 1 kW"[VS04]. In 18th century James Watt created steam engine. Afterward, even more complex devices, tools, and vehicles were created and invented. Currently, the primary goal of numerous researchers centers around the acquisition, efficient storage, and utilization of electrical energy.

Increasing concerns about pollution from fossil fuel engines and potential shortages of petrol, together with the continuing rise in prices are forcing the current vehicle market to find new market to find new alternatives to reduce the use of fossil fuels consumption [YW12], [Cha93], [Cha02]. This is the reason for the major development in the hybridization of vehicle powertrains [YW12], [ELR08], [KM97], [MERE99]. The International Energy Outlook 2023 (IEO2023) Reference case projects growth in transportation-sector energy consumption over the 28 years from 2022 to 2050 between 8% and 41% [U.S23a]. Due to current policy incentives, efficiency standards, and decreasing battery costs, electric vehicle (EV) sales are growing and projected to grow [U.S23b]. Because of this, the share of electric energy in the total energy consumption in the transportation sector can also be expected to grow. One of the benefits of EVs in comparison to fossil-fuel-powered vehicles is regenerative braking. The electrical current produced by the system is directly proportional to the level of braking force applied. This means the stronger the braking force, the greater the electricity generated. With regenerative braking, up to 70% of kinetic energy can be recovered from the vehicle's acceleration [Bor13], [FAR16]. Another reason to focus on energy efficiency is to minimize the adverse effects of human factors, such as aggressive braking, high-speed driving, inefficient acceleration and deceleration, improper tire maintenance, and more. Additionally, a system with torque vectoring and traction control can increase stability and safety[YW12]. This thesis can also address the issue of wheel sway, which is the lateral motion or side-to-side movement of a vehicle's wheels. This can decrease the vehicle's stability and handling, causing uneven tire wear and other problems. From an energy standpoint, tire wear and rolling resistance caused by lateral oscillations can increase energy loss. Asymmetrical torque distribution can improve cornering stability, reducing the likelihood of lateral oscillations. Path tracking aims to maintain the vehicle on a desired path, reducing lateral deviation and avoiding erratic lateral movements to return to the path.

Overall, the phenomenon of EVs and electric mobility in general is a compelling topic of discussion. Therefore, this thesis deals with the energy efficiency of electric vehicles.

■ 1.2 Presented Approach

In this thesis, we focus on the development of a sufficient power evaluation methodology. We obtain power from generalized forces, torque and velocity of the vehicle and of the wheels. This allows us to evaluate the efficiency and analyze the driving resistance of the vehicle and wheels for different driving scenarios and quantify the isolatable or controllable factors such as aerodynamics, friction, and rolling resistance. For the purposes of this thesis, the twin-track model is used for the description of our vehicle. This model

is implemented with the help of a book from Dieter Schramm [DS14], Tire and Vehicle Dynamics by Hans B. Pacejka [Pac05], and Vehicle Dynamics and Control written by Rajesh Rajamani [Raj12]. A low-level control system is implemented, which includes traction control and asymmetric traction moment distribution, also known as Torque Vectoring (TV). Further a high-level control system which objective is path tracking was designed.

◼ 1.3 Goal

The outcome of this thesis shall propose algorithms for energy efficiency evaluation of vehicle maneuvers. The development of vehicles with electric powertrains and corner modules opens new possibilities for path-tracking strategies.

1. Get familiar with vehicle dynamic mathematical models and implement suitable ones.

2. Get familiar with path-tracking algorithms.

3. Develop and implement a methodology for energy evaluation of over-actuated vehicles.

4. Develop algorithms testing

◼ 1.4 Thesis structure

Chapter 2 State of the Art
This chapter contains some background technical information to each partial sub-problem of the thesis. It defines the over-actuated vehicle and explains the terms torque, vectoring, path tracking, and power efficiency. Moreover, it analyzes the previous works and research conducted on our problem.

Chapter 3 Mathematical Vehicle Models
Here, the further used kinematic model and twin-track model are described with corresponding equations. Pacejka's tire model is also presented for the twin-track model. Identification of a model is discussed.

Chapter 4 Architecture Design In this section, the structure of the architecture of the framework and the controllers is explained. Also, the generation of the reference path is described.

Chapter 5 Low-level Control

In this chapter, the torque vectoring system and traction control system are presented as a low-level control system with a detailed focus on the feedback controllers and the torque distribution.

Chapter 6 High-level Control
Development of path tracking is the main objective of this chapter and is presented as a high-level control algorithm.

Chapter 7 Power Evaluation
Our methodology for energy evaluation of over-actuated vehicles is explained here. The assumptions made, and the choice of strategies for further simulations are presented and described here as well.

Chapter 8 Conclusion
In the last chapter, the achieved results are summarized, and ideas for future work are discussed.

Chapter 2

State of the Art

2.1 Power efficiency

Power efficiency is a currently widely discussed topic. Numerous companies, universities, and other institutions are researching this area. The trend in the automotive industry is to shift from gas-powered to electric vehicles. Due to the crisis and rising electricity prices, there is a growing need to improve the efficiency of electric vehicles. As mentioned earlier 1.1, the share of electric energy in the transportation and automotive industry is expected to increase, and thus, working on improving the efficiency is topical.

Energy losses of vehicles or electric vehicles have different causes. Firstly, the energy losses can be decreased by constructing "the most power-efficient car", focusing on components of chassis, powertrain, drivetrain(s), suspension, and tires. The design of the shape of the vehicle can reduce the aerodynamic drag. The usage of suitable powertrain for the vehicle's purposes. The choice of tires can influence the rolling resistance, traction, wear resistance, temperature sensitivity, and weight, which are all factors that have an impact on energy efficiency.

Similarly, it is possible to review all other components, such as motors, batteries, suspension, weight distribution, etc. Although the vehicle may be engineered to minimize power losses and achieve desired performance, it might not be the most optimal system in the end. Even if it were, the construction of such a vehicle could be expensive, and it would not be widely used or produced. For the overall reduction of energy losses, it might be more desirable to construct a vehicle with slightly less efficient components that are more affordable and accessible to the masses. Moreover, besides the focus on construction, the efficiency of the drive can still be improved by executing driving maneuvers more effectively. The task of maneuvering belongs partly

to the path tracking problem, so it is the topic of the next section.

▉ 2.2 High-level control

In autonomous vehicles, path tracking is one of the research objectives. The aim is to control both the longitudinal and lateral directions to follow a reference path. Generally defined in the field of Robotics and Automation, a path is a sequence of positions between an initial and final position without time parameterization. A trajectory is a path with time constraints. Instead of time parameterization, a reference path can be given a reference velocity or acceleration. The reference path has to be generated, which can be done by algorithms based on Rapidly-exploring Random Trees (RRT), A*, Dijikstra's algorithm, Sample algorithm or others. This problem is not one of the objectives of this thesis; that is why the algorithms to solve this problem are only briefly mentioned without further explanation.

Nowadays, many path-tracking algorithms, such as the Dynamic Window Approach and Pure Pursuit algorithm, are used to navigate vehicles to follow a given path. Quite known is Model Predictive Control, which calculates the prediction of the future behavior of the vehicle and optimizes the control input over a prediction horizon [Šv23]. Alternatively, the Lateral and Longitudinal Control Decoupling approach divides the longitudinal control (acceleration, breaking) and lateral control (steering angles) [Mac23]. Stanley Controller is an algorithm that uses cross-track and heading errors to control the steering angles of the wheels. The approach in this thesis uses the same errors to control the lateral motion of the vehicle.

The redundancy of the vehicle is also partly connected to the high-level control and can influence energy efficiency. A vehicle with the possibility of steering with all four wheels (See Fig. 2.1) has redundancy in control, allowing more flexibility and better maneuvering. However, a vehicle with fixed rear wheels would be cheaper, so such a vehicle's energy improvement is desirable. This is also the configuration used in this thesis. With only two wheels capable of steering, the goal is to minimize the driving resistance. For this reason in this thesis the kinematic model is used as a reference model, since the kinematic model neglects sideslip angles, which might be for specific scenarios significant and may influence the path tracking by bringing inaccuracies and disturbances.
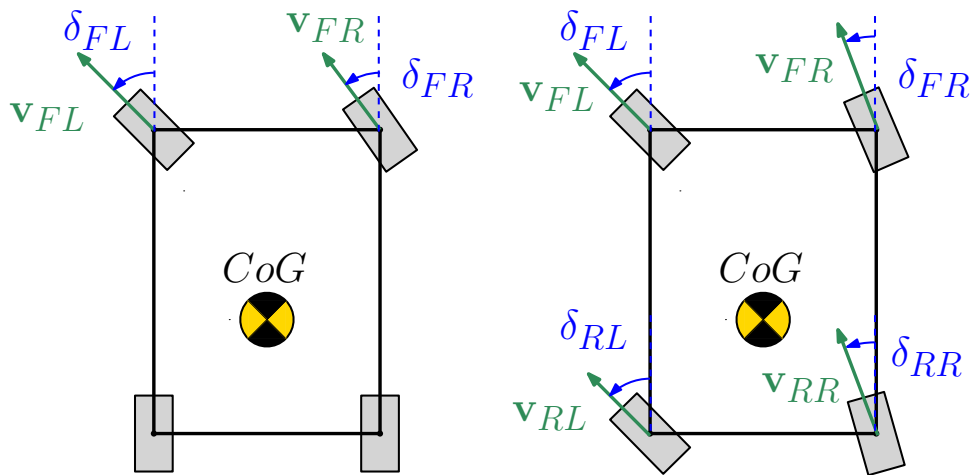
Figure 2.1: Vehicle with a) with only front steering wheels and b) with all four steering wheels

2.3 Over-actuated vehicles

Another way of redundancy is redundancy in actuation. An over-actuated system has more ways of actuation per particular DoF. In simple terms, when controlling an over-actuated vehicle, the system has more actuators than are strictly necessary to control its motion. The vehicles with more drivetrains each, each wheel is for movement in a 2D plane, an over-actuated vehicle. "The use of electric power also facilitates drive train design to have various possible configurations, thus enhancing the driving performance and improving integration and safety 2.2 shows four possible drive train configurations with different motor positioning: where each topology has its advantages and disadvantages with respect to performance, safety, reliability, and cost" [YW12]. Having two or four drivetrains is an advantage for more efficient traction control and torque vectoring, which is described below as a low-level control system. A vehicle with all four wheels capable of steering has a potential for over-actuation, since each wheel can contribute to steering.
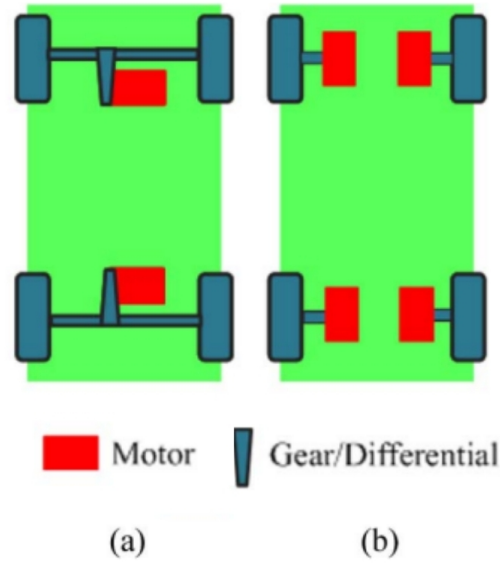
Figure 2.2: Two possible drive train architectures. (a) Both front wheel and rear wheel driven. (b) Four-wheel driven.[YW12]

2.4 Low-level control

The low-level control system is in the context of this thesis system, which consists of Traction Control (TC)/ λ-Control and asymmetric distribution of torque. In this thesis is this system usually called Torque Vectoring (TV) or low-level control system.

Torque vectoring belongs among the active vehicle control systems, alongside Anti-Lock Braking System (ABS), Anti-Slip Regulation (ASR) and Electronic Stability Program (ESP). It controls the distribution and asymmetric transfer of engine torque to left and right driven wheels, allowing cornering torques to be different on right and left wheels (See Fig. 2.3). This system can have the ability to divide torque between only two wheels (left/right), which is less complex because the front-wheel drive differential only needs to differentiate between two wheels and monitor steering angle and angular velocity as varying factors during driving. The drive exerting different forces on the wheels when these factors change during the drive. The same applies to the rear-wheel drive differential. Typically, the TV system is utilized for all-wheel drive automobiles. The differential distributes torque between the right and left wheels, as well as between the front and rear wheels, independently. The significance of TV system development has escalated, particularly with the growing use of electric vehicles. This is due to the fact that electric vehicles, with two or four drivetrains (See Fig. 2.2), can make torque vectoring even more precise. The objective of the TV is to manage

8

the lateral dynamics and stability of the vehicle, particularly in challenging conditions, while also enhancing the vehicle's maneuverability to reduce the driver's effort in steering, thereby maximising comfort [DNSG14], [Mut12], [PLRG10], [FKF^{+}13].

Despite sharing similar aims as ESP, torque vectoring is utilised in diverse scenarios, often not critical, in contrast to other active vehicle control methods previously mentioned. ESP is typically used to take control of a vehicle in hazardous situations where the vehicle, driver or passengers may be at risk of injury. To avoid interference with the control demands of ESP, the TV must be turned off when ESP is in control. Whilst ESP is specially designed to manage critical situations, the aim of the TV is to prevent them. Also both λ control and ABS are also utilised for control of vehicle's longitudinal acceleration and are dependent on longitudinal traction force of tire slip ration λ[Tur19].
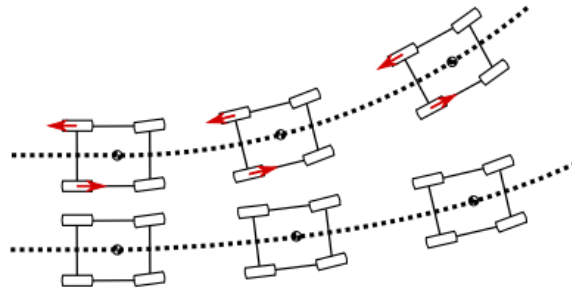
Figure 2.3: Torque Vectoring working on rear axle, where the torques difference on rear wheels is indicated by red arrow [Tur19]

9

Chapter 3

Mathematical vehicle models

3.1 Introduction

For the development of path tracking algorithms and control algorithms, simplified models of the vehicles are used as they sufficiently describe the vehicle's motion. This chapter provides an overview of all the other vehicle models that are be used. The accuracy of the dynamics model is essential for further developing autonomous vehicle control algorithms and torque vectoring systems, both of which are the main objectives of this thesis.

The kinematic model is the reference model, providing the most straight-forward mathematical description of the vehicle's motion. The nonlinear twin-track model is used to describe the vehicle and to develop a torque vectoring system

3.2 Coordinate systems

From the definition from ISO 8855 [Int11] "the reference frame is geometric environment in which all points remain fixed with respect to each other at all times. An inertial reference frame is assumed to have zero linear and angular acceleration and zero angular velocity. An axis system is set of three orthogonal directions associated with X, Y and Z axes, where for right-handed axis system is assumed that $Z = X \times Y$. A coordinate system (CS) numbering convention used to assign a unique ordered trio (x, y, z) of values to each point in a reference frame, and which consists of an axis system plus an origin point."

■ 3.3 Local coordinate systems

Local coordinate systems are typically associated with specific objects, in our case, a vehicle, in comparison to global coordinate systems. In the field of vehicle navigation, control systems, and positioning of objects within a limited area, local reference frames are commonly used. These frames include the North-East-Down (NED), East-North-Up (ENU), SAE J670e, and SAE J1930 coordinate systems. The SAE coordinate systems are widely used in the field of automotive engineering.

NED and ENU serve as local tangent plane systems utilized as external earth-fixed reference frames, originating at a specific point of interest on Earth. This approach assumes a flat Earth surface, allowing the use of the Cartesian coordinate system. An ellipsoidal model is employed to approximate the Earth's surface, and the axes are tangentially aligned to it. For the NED coordinate system, the X-axis is oriented to the North, the Y-axis to the East, and the Z-axis points downwards in line with the tangent plane's normal. In contrast, the ENU coordinate system positions the X-axis towards the East, the Y-axis towards the North, and the Z-axis perpendicular to the tangent plane, pointing upwards[Šv23].
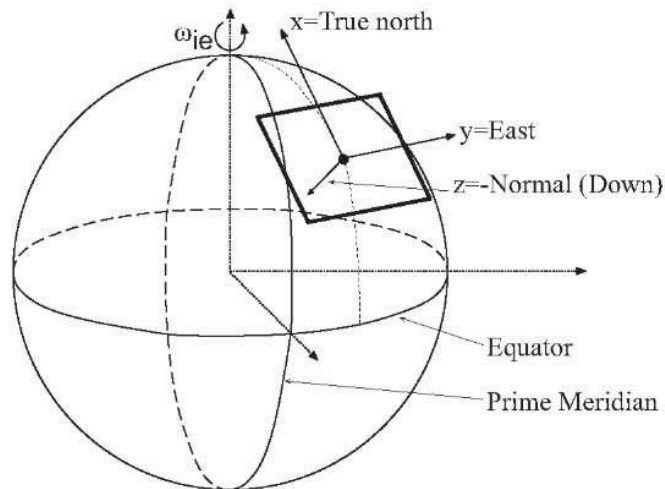
Figure 3.1: Local Geodetic frame, which is determined by adding a tangent plane to specific point on the Earth's surface[MB16]

■ 3.4 Vehicle coordinate systems

In this thesis we consider the vehicle coordinate system shown in Fig. 3.2.
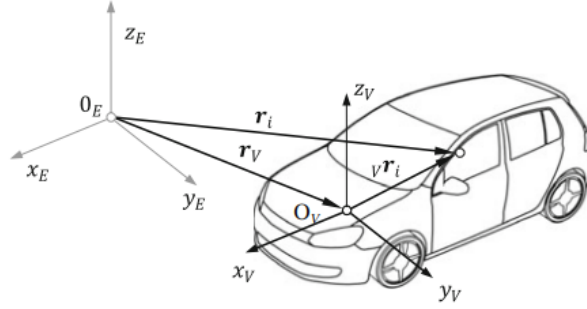
Figure 3.2: Inertial (earth-fixed) coordinate system and Vehicle (body-fixed) coordinate system. Adopted from [DS14]

▉ 3.5 Kinematic model

In this section, the kinematic model of the motion of the vehicle is introduced. This model is obtained from the Ackermann steering geometry of the vehicle and describes the motion without considering the forces that generate the motion. The models were described based on [Han23],[Mac23] and [Mon18].

With an Ackermann steering geometry, the steering angle at the left and right (inner and outer) wheels is different because the radius to the center of rotation (O) is different. This is shown in Fig.3.3a and described by the equation 3.1.

$$\cos(\delta_r) - \cos(\delta_l) = \frac{d}{L} \tag{3.1}$$

The kinematic model is the bicycle model, meaning that the two front and two rear wheels are represented by only one wheel in the center of the axle (see Fig.3.3b). This could be achieved by having the wheels move along concentric circular paths when stationary, aligned with the tangents of the circle, and with no lateral slip during the movement.

As we can see, the model shown in Figure 3.3b as a bicycle model neglects the fact that the steering angles of the right and left wheels are different. The wheel angle is then calculated using Eq. 3.2.

$$\tan^{-1}(\delta_F) = \frac{\tan^{-1}(\delta_{FL}) + \tan^{-1}(\delta_{FR})}{2} \tag{3.2}$$

From the equation 3.2, the steering angles on the front left front right wheel can be derived:

$$\delta_{FL} = \tan(\tan^{-1}(\delta_F - \frac{d}{2L}), \tag{3.3}$$

$$\delta_{FR} = \tan(\tan^{-1}(\delta_F + \frac{d}{2L}). \tag{3.4}$$

13

Therefore, as described by the equation 3.5, δ_F can be approximated as the average of the steering angles of the left and right wheels. The same rule applies to the front wheel as well as to the left wheel.

$$\delta_F \approx \frac{\delta_{FL} + \delta_{FR}}{2} \tag{3.5}$$

(a) : A front wheel steering vehicle and steering angles of the inner and outer wheel [Mac23]

(b) : Equivalent bicycle model for a front wheel steering vehicle [Mac23]
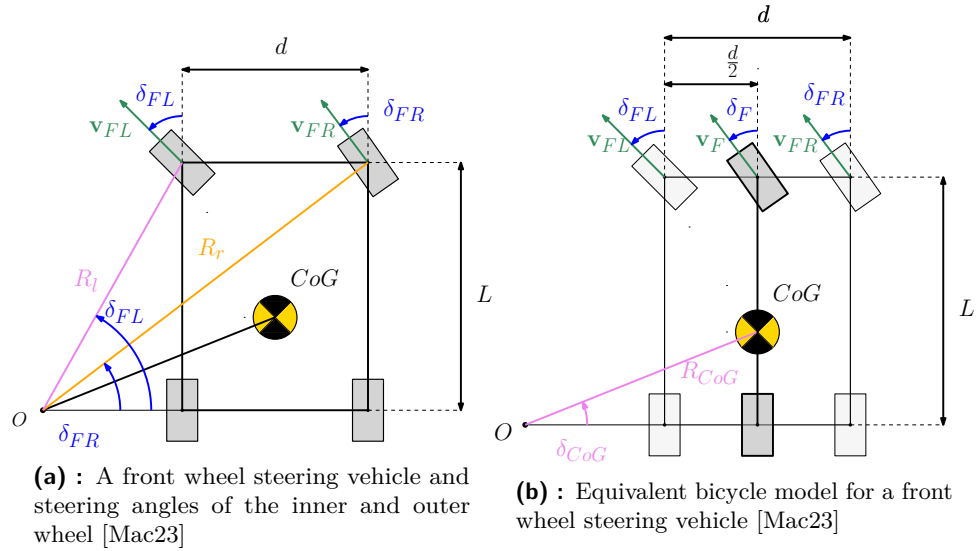
Figure 3.3: Ackermann geometry

- L is the length of the wheelbase of the vehicle

- d is the track width of the vehicle

- δ_{FL} and δ_{FR} are the steering angles of front left and front right wheels respectively

- $\vec{v}_{FL}$ and $\vec{v}_{FR}$ are the velocities of the front left and front right wheels, respectively

- R_l, R_r are the radii of rotation of the front left and front right wheel, respectively

The main advantage of this model is its simplicity. Many constraints and assumptions must be made to achieve these simplified equations. The first and most important assumption is that there is no lateral slip of the wheels during the vehicle's movement. Thanks to this assumption, velocity vectors of the front and rear wheel are aligned with the x-axis of the wheel as it is shown in Fig 3.4.
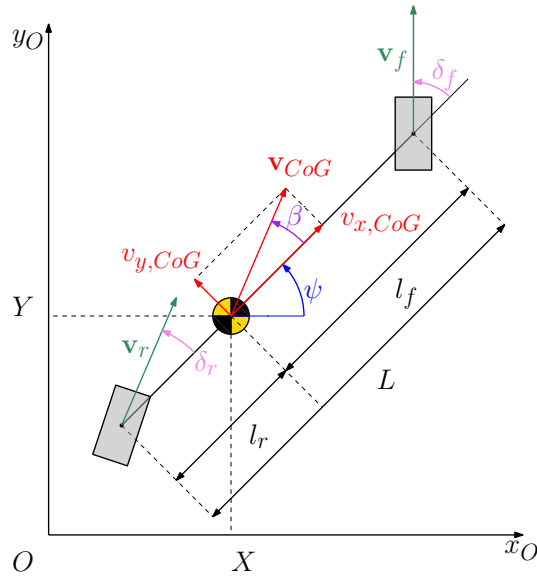
Figure 3.4: Kinematic model in coordinate system O[Mac23]

In addition, the total lateral force F_y acting on the vehicle of mass m generated by the two tires moving on a circle of radius R with velocity v_{CoG} is equal to

$$F_y = \frac{mv_{CoG}^2}{R}. \tag{3.6}$$

This assumption is only valid for maneuvering at low speeds and small steering angles; the model must be more accurate for more aggressive maneuvering at higher speeds or larger steering angles. This thesis's primary purpose is validation and generating reference signals for torque vectoring.

This vehicle model is designed to operate within a 2D plane, with no consideration for vertical movement. The model conceptualizes the vehicle as a line segment with three degrees of freedom, effectively described by three primary coordinates in the global coordinate system (NED) illustrated in Fig. 3.4. The positions of the center of gravity along the North (N) and East (E) axes are denoted by X and Y, respectively. The orientation of the vehicle, referred to as the yaw angle, is denoted by ψ.

The following equations describe changes to the position and orientation of the vehicle while moving in the plane. This is accomplished by incorporating factors such as velocity, yaw rate, side slip angle, distances between axles, and steering angles. Technical abbreviations will be explained upon their first occurrence.

$$\dot{X} = v_{CoG}\cos(\psi + \beta) \tag{3.7}$$

$$\dot{Y} = v_{CoG}\sin(\psi + \beta) \tag{3.8}$$

15

$$\dot{\psi} = \frac{v_{CoG}\cos\beta}{l_f + l_r}\left(tan(\delta_f) - tan(\delta_r)\right) \tag{3.9}$$

$$\beta = \tan^{-1}\left(\frac{l_f\tan(\delta_r) + l_r\tan(\delta_f)}{l_f + l_r}\right). \tag{3.10}$$

- X and Y represent the vehicle's center of gravity position in the global coordinate system.

- ψ is the vehicle's yaw angle, indicating its orientation or heading.

- $\dot{\psi}$ is the vehicle's yaw rate, which is the change in the yaw angle over time.

- v_{CoG} is the magnitude of the velocity vector at the vehicle's center of gravity (See Fig. 3.4).

- β is the side slip angle of the vehicle.

- L is the total wheelbase of the vehicle, which is the sum of l_f and l_r.

- δ_r and δ_f are the steering angles of the rear and front wheels, respectively.

▨ 3.6 Twin-track model

The subsequent section focuses on the 10-state spatial twin-track model without any suspension kinematics and without any powertrain modeling, chosen for its adequate convenience in fulfilling the objective of this thesis, as the single-track model is not suitable for our low-level control. The model is used to validate the low-level and high-level control systems, both of which are explained in later chapters 5 and 6. For modelling of this model presented sources were used [DS14], [VH23] and [Cib19]. The model can be divided into four parts, as shown in Fig. 3.5. The front and rear wheels are not represented by a single wheel in the center of the axle, as in the kinematic or single-track model. Instead, they are represented separately, as shown in figures 3.5 and 3.6. Each wheel is connected to the vehicle at its pivot point.
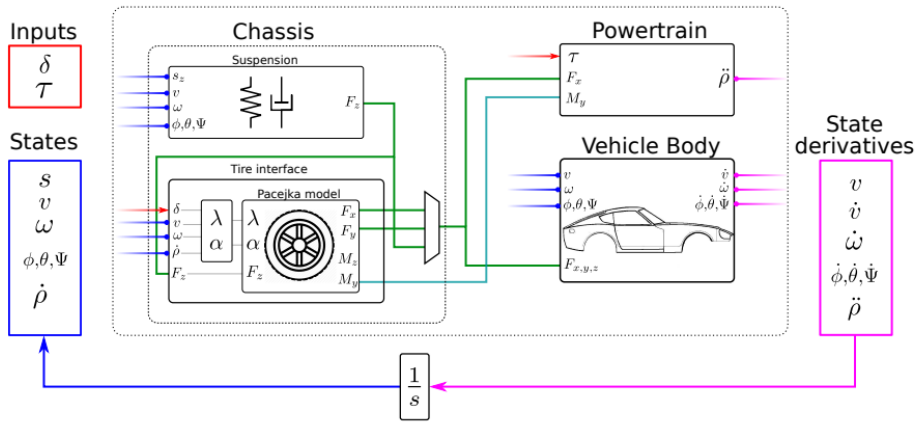
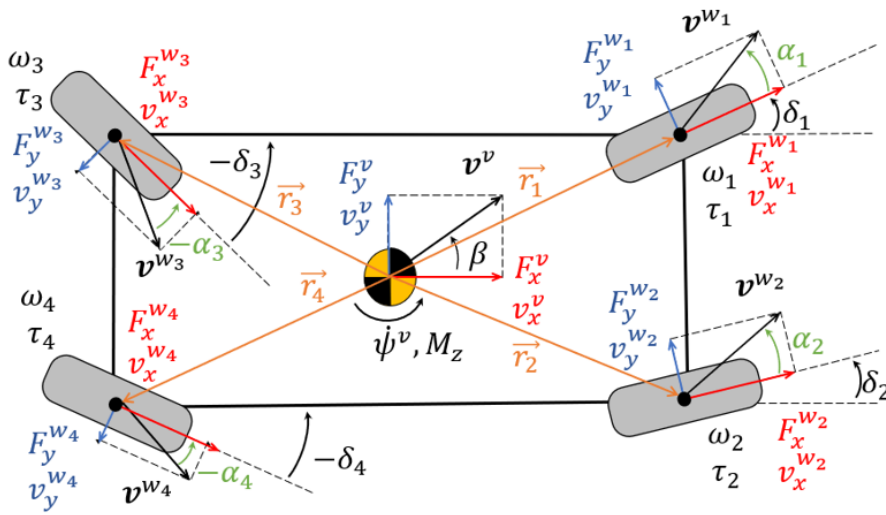**Figure 3.5:** Scheme of the twin-track model. Adopted from [Cib19]

Figure 3.6: Top view of the vehicle twin-track model. Adopted from [Han23]

As mentioned earlier, this model does not include any suspension kinematics, which means that the wheels are directly connected to the vehicle chassis by the spring and damper forces, which are stamping forces. The model cannot be used to analyze the impact of the camber or other spatial movements of the wheels [DS14]. However, for our purposes, the model is sufficient. The model has $f = 10$ DoF.

■ 3.6.1 Vehicle body

The vehicle's body can be described with Newton's and Euler's equations. The Newton equations for the chassis in vector form are:

$$m\mathbf{a}^V = \mathbf{F}^V \tag{3.11}$$

$$m\left(\dot{\mathbf{v}}^V + \boldsymbol{\omega}^V \times \mathbf{v}^V\right) = \mathbf{F}^V \tag{3.12}$$

$$m\left(\begin{bmatrix} \dot{v}_x^V \\ \dot{v}_y^V \\ \dot{v}_z^V \end{bmatrix} + \left(\begin{bmatrix} \omega_x^V \\ \omega_y^V \\ \omega_z^V \end{bmatrix} \times \begin{bmatrix} v_x^V \\ v_y^V \\ v_z^V \end{bmatrix}\right)\right) = \mathbf{F}^V \tag{3.13}$$

$$m\mathbf{a}^V = \sum_{i=1}^{4} \mathbf{T}_V^{w_i} \cdot \mathbf{F}^{w_i} + \mathbf{F}_g^V + \mathbf{F}_{res}^V \tag{3.14}$$

$$m\mathbf{a}^V = \sum_{i=1}^{4} \mathbf{T}_V^{w_i} \cdot \begin{bmatrix} \mathbf{F}_x^{w_i} \\ \mathbf{F}_y^{w_i} \\ \mathbf{F}_z^{w_i} \end{bmatrix} - \frac{1}{2}c_{res}\rho A(v_x^V)^2 + \mathbf{T}_E^V \begin{bmatrix} 0 \\ 0 \\ -m^V g \end{bmatrix} \tag{3.15}$$

- $\mathbf{F}^V$ is a vector of the total force acting on the body of the vehicle at the center of gravity.

- $\mathbf{F}_x^{w_i}$, $\mathbf{F}_y^{w_i}$, $\mathbf{F}_z^{w_i}$ are forces acting on the vehicle at the center of gravity along the x-, y-, z-axes, respectively. They are presented in body-fixed coordinates and are partial components of $\mathbf{F}^V$.

- The term

$$-\frac{1}{2}c_{res}\rho A(v_x^V)^2$$

  in equation 3.15 is known as the drag force formula and describes air resistance. The c_{res} is the aerodynamic drag coefficient, ρ is the density of the fluid (air in our case), A is the cross-sectional area of the vehicle, and v_x^V is the longitudinal velocity in center of gravity. The air resistance is presented here but not used in the implemented model.

- The force $\mathbf{F}_g^V$ presented in equation 3.14 is a gravitational force acting in the direction opposite to the positive direction of the z-axis and can be further described as

$$\mathbf{F}_g^V = mg\mathbf{e_z}.$$

- In equation 3.14, the force $\mathbf{F}^V_{res}$ is a collection of all the resistant and aerodynamic forces and drag and can be further described as

$$\mathbf{F}^V_{res} = -\frac{1}{2}c_{res}\rho A(v^V_x)^2$$

- $\mathbf{T}^{\mathbf{E}}_{\mathbf{V}}$ is a transformation matrix that transforms the earth-fixed gravitational acceleration to body-fixed coordinates [DS14] [Cib19].

- $\mathbf{T}^{\mathbf{i}}_{\mathbf{V}}$ is the identity transformation that transforms the vector i-th wheel-fixed CS to vehicle body-fixed frame

The Euler's equations for the chassis in vector form are:

$$\Theta^V \begin{bmatrix} \dot{\omega}^V_x \\ \dot{\omega}^V_y \\ \dot{\omega}^V_z \end{bmatrix} + \begin{bmatrix} \omega^V_x \\ \omega^V_y \\ \omega^V_z \end{bmatrix} \times \left(\Theta^V \begin{bmatrix} \omega^V_x \\ \omega^V_y \\ \omega^V_z \end{bmatrix} \right) = \mathbf{T}^V$$

$$\Theta^V\dot{\boldsymbol{\omega}}^V + \boldsymbol{\omega}^V \times \left(\Theta^V\boldsymbol{\omega}^V \right) = \sum_{i=1}^{4} \mathbf{r}^V_{w_i} \times \begin{bmatrix} \mathbf{F}^{w_i}_x \\ \mathbf{F}^{w_i}_y \\ \mathbf{F}^{w_i}_z \end{bmatrix} + \mathbf{r}^V_{res} \times \mathbf{F}^V_{res} \qquad (3.16)$$

- Θ^V is the inertia matrix of the vehicle in the vehicle-fixed frame.

- $\boldsymbol{\omega}^V$ is the angular velocity vector of the vehicle in the vehicle-fixed frame.

- $\mathbf{T}^V$ is the torque vector acting on the vehicle in center of gravity in the vehicle-fixed frame.

- Θ^V is the inertia matrix of the chassis in the vehicle-fixed frame.

- $\dot{\boldsymbol{\omega}}^V$ is the angular acceleration vector of the chassis in the vehicle-fixed frame.

- $\boldsymbol{\omega}^V$ is the angular velocity vector of the chassis in the vehicle-fixed frame.

- $\mathbf{r}^V_{w_i}$ is the position vector from the center of mass to the i-th wheel.

- $\mathbf{F}^{w_i}_x, \mathbf{F}^{w_i}_y, \mathbf{F}^{w_i}_z$: are the forces acting on the i-th wheel in the vehicle-fixed frame.

- $\mathbf{r}^V_{res}$ is the position vector from the center of mass to the point where the force $\mathbf{F}^V_{res}$ is acting.

3.6.2   Chassis

Suspension

For this thesis, the suspension of the vehicle needs to be addressed, as it is not necessary to consider the suspension in this model for this thesis.

■ Tire interface

This section defines the slip variables used by the tire models based on [Raj12] [Pac05] [DS14]. For path tracking, the generation of lateral force is important, and for braking or acceleration, the generation of longitudinal force is essential. The generation of the longitudinal force is dependent on traction, engine power, breaking, surface conditions, and weight transfer. The generation of the lateral force depends on the tire contact patch, determined not only by tire dimensions but also by the vertical load and inflation pressure. The adhesion of the two surfaces generates the force. The adhesion depends mainly on road surface conditions as the surface can be icy or wet[VH23].

The slip ratio λ (See Eq. 3.17) and slip angle α (See Eq. 3.18) are the slip variables used to describe wheel forces generated at tire-to-road interface. The notation of this section is slightly different from [DS14], especially since the slip angle is denoted by λ instead of s.

$$\lambda_{w_i} = \frac{r_{w_i}\omega_{w_i} - v^{w_i}}{max(|v^{w_i}|, |r_{w_i}\omega_{w_i}|)} \quad ,\text{where } \lambda_{w_i} \in [-1, 1] \qquad (3.17)$$

$$\alpha_i = -\arctan\left(\frac{v_y^{w_i}}{|v_x^{w_i}|}\right) \qquad (3.18)$$

- ■ $v_x^{w_i}$ and $v_y^{w_i}$ are velocities of the i-th wheel center point along x or y axis respectively in the wheel-fixed coordinate system.

- ■ ω_{w_i} is angular velocity of the wheel.

- ■ r_{w_i} is the radius of i-th wheel.

■ 3.6.3 Tire models

The following models simulate the behavior of tires under different conditions and loading scenarios. The level of accuracy and complexity varies, with the simplified Pacejka model being the simplest and the full Pacejka model providing a more comprehensive and accurate depiction of tire behaviour. Finally, the introduction of a friction ellipse in the simplified model is likely a means of addressing the interdependence of lateral and longitudinal forces [Pac05][DS14][VH23] and [Raj12].

■ Full Pacejka

The full Pacejka tire model is a more comprehensive representation of tire behavior. It includes a broader range of parameters for various real-world tire
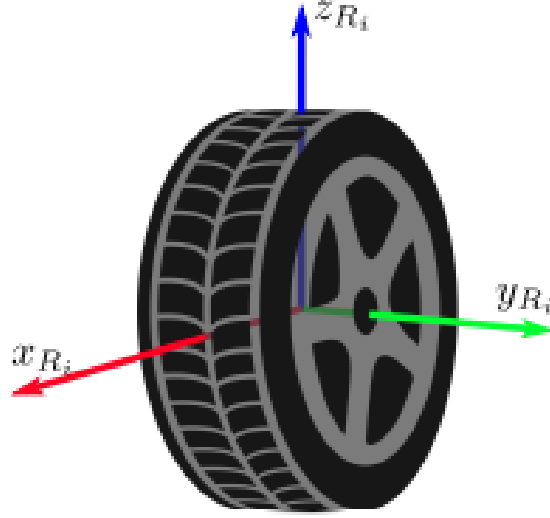
Figure 3.7: Tire coordination system [Mon18]

behaviors such as slip angle, longitudinal slip, and camber angle[Pac05][Cib19]. Since this model is more accurate, it is also more difficult to obtain and many experiments must be done to obtain the necessary data for proper fitting. Therefore, only the simplified version is used in this thesis.

■ Simplified Pacejka Formula

The lateral and longitudinal forces (F_x and F_y) are not entirely independent in the real world. This interdependence is often expressed using a friction ellipse. Additional considerations are introduced to account for this dependence, still using the simplified Pacejka model as a basis [Pac05].

The Simplified Pacejka Model employs coefficients B, C, D, and E within the framework of the Magic formula:

$$F = D \cos \left(C \arctan \left(Bx - E \left(Bx - \arctan(Bx) \right) \right) \right) \qquad (3.19)$$

Here, the variable x can denote the sideslip angle α or longitudinal slip λ. The tire force F can take on one of three forms: F_y, T_z, or F_x, depending on the input argument x and the set of coefficients B, C, D and E, where B is the stiffness factor, C the shape factor, D the peak value and E the curvature factor. To calculate the longitudinal force (F_x, for instance), x is replaced with λ, while for F_y and T_z, α is used.

In reality, the coefficients B, C, D, and E are time-variant and contingent on the specific physical interpretation of F. However, in this simplified model,

these coefficients are held constant for a given type of force (F_y, T_z, or F_x). Thus, three sets of these parameters are required to calculate each of these forces (F_y, T_z, and F_x).

It is important to note that this approach treats the forces F_x and F_y as independent. In reality, this independence does not hold. The interdependence between these forces is often visualized using a traction ellipse, also known as a friction ellipse or Kamm's circle [Pac05].
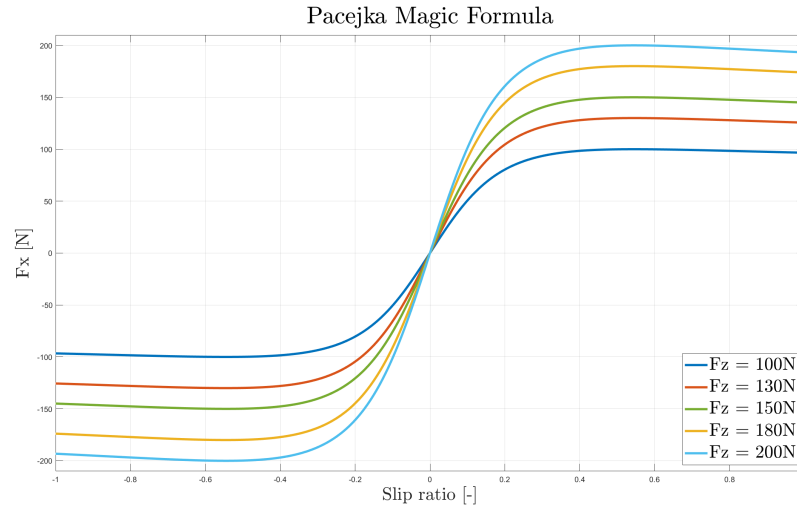
Figure 3.8: Pacejka Magic formula for given normal forces

■ Kamm's circle

The tire's ability to generate forces F_x and F_y is not unlimited. There is a limit to these forces, and this limit is commonly referred to as Kamm's circle, although it is sometimes referred to as the friction ellipse, as shown in Fig. 3.9. This constraint becomes particularly relevant when a vehicle is simultaneously cornering, accelerating, or decelerating. The algorithm for calculating and applying these force limits is usually taken from a referenced source.
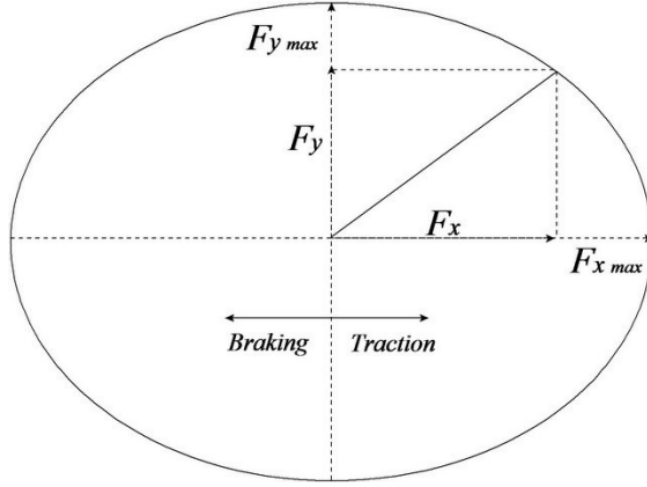
Figure 3.9: Kamm traction ellipse

$$\alpha^* = \sin(\alpha) \tag{3.20}$$

$$\beta = \arccos\left(\frac{|\lambda|}{\sqrt{\lambda^2 + \alpha^{*2}}}\right) \tag{3.21}$$

$$\mu_{x,act} = \frac{F_{x,0}}{F_z} \quad \mu_{y,act} = \frac{F_{y,0}}{F_z} \tag{3.22}$$

$$\mu_{x,\ max} = \frac{D_x}{F_z} \quad \mu_{y,\ max} = \frac{D_y}{F_z} \tag{3.23}$$

$$\mu_x = \frac{1}{\sqrt{\left(\frac{1}{\mu_{x,act}}\right)^2 + \left(\frac{\tan(\beta)}{\mu_{y,max}}\right)^2}} \tag{3.24}$$

$$\mu_y = \frac{\tan(\beta)}{\sqrt{\left(\frac{1}{\mu_{x,max}}\right)^2 + \left(\frac{\tan(\beta)}{\mu_{y,act}}\right)^2}} \tag{3.25}$$

$$F_x = \frac{\mu_x}{\mu_{x,act}} F_{x,0} \tag{3.26}$$

$$F_y = \frac{\mu_y}{\mu_{y,act}} F_{y,0} \tag{3.27}$$

- α^*: sideslip angle of the tires.

- β: the sideslip angle of the vehicle.

- $\mu_{x,\text{act}}$: longitudinal tire friction coefficient in the active region, given as the ratio of longitudinal force $F_{x,0}$ to vertical load F_z.

- $\mu_{y,\text{act}}$: lateral tire friction coefficient in the active region, given as the ratio of lateral force $F_{y,0}$ to vertical load F_z.

- $\mu_{x,\text{max}}$: maximum longitudinal tire friction coefficient, given as the ratio of D_x to vertical load F_z.

- $\mu_{y,\text{max}}$: maximum lateral tire friction coefficient, given as the ratio of D_y to vertical load F_z.

- μ_x: effective longitudinal tire friction coefficient.

- μ_y: effective lateral tire friction coefficient

- F_x: longitudinal force action on the tire

- F_y: Lateral force acting on the tire

■ Bilinear

The Pacejka magic Formula can be approximated. The bilinear approximation takes small range of slip ratios, where the tire behaviour is approximately linear.

■ 3.7 Powertrain

The powertrain or any of the vehicle's drivetrains have not been modeled in this thesis as they are not needed for the purposes of this thesis. In the powertrain or drivetrain, the time constant is affected by several factors, including the inertia of rotating components, the stiffness of the powertrain/drivetrains, and damping effects. Neither the stiffness nor the time constants of the powertrain or of the drive trains are taken into account.

■ 3.8 Vehicle platform

The twin track model is to represent this vehicle platform, which is currently being developed at the Department of Control engineering by the Smart Driving Solutions research team at the Czech Technical University in Prague. The model of the vehicle is shown in the Fig. 3.10 and the parameters which were used are in the Table 3.1.
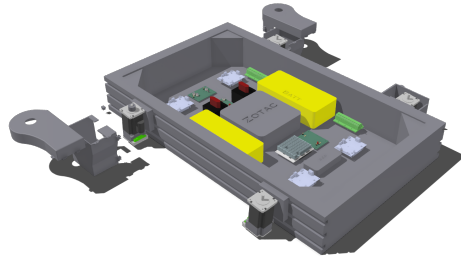
Figure 3.10: The future expected validation platform

Parameters of the twin-track model		
l_f [m]	0.48	Distance between CoG and the center of the front axle
l_r [m]	0.35	Distance between CoG and the center of the rear axle
d [m]	0.735	Track width
m [kg]	63.8	Mass of the vehicle
I_z [kg·m^2]	11.15	Moment of inertia of the vehicle
I^w [kg·m^2]	0.039	Moment of inertia of the wheels
r [m]	0.15	Radius of the wheels

Table 3.1: Parameters of the twin-track model for this platform.

Chapter 4

Architecture design

This chapter describes the architecture. As our thesis aims to create a torque vectoring system and path tracking algorithm, we needed to decouple the lateral and longitudinal dynamics. The low-level part of our architecture deals with the longitudinal dynamics, while the high-level part deals with the lateral dynamics. To validate the designed control systems, we created a simulation framework as our primary tool.

4.1 High-level and low-level control separation

The motion of a vehicle consists of both lateral and longitudinal motions. Presented low-level control system focus on the traction control and its asymmetric distribution. The high-level control system focus on path tracking.

To achieve greater efficiency and better results, the dynamics of these movements are decoupled by separating their modeling and control. This is done based on certain assumptions, such as the absence of a time or speed reference since the task is path tracking and not trajectory tracking. As a result, the wheel torques can be controlled externally.

4.2 Simulation Framework

This chapter will introduce the simulation framework used for performing the simulation experiments. The framework was developed using Matlab version R2022b, a software from MathWorks company, and its toolbox Simulink.

■ 4.2.1   Framework structure

This section presents a description of the structure of our framework. The Fig. 4.1 shows a simple schematic of the architecture. The block are described below.
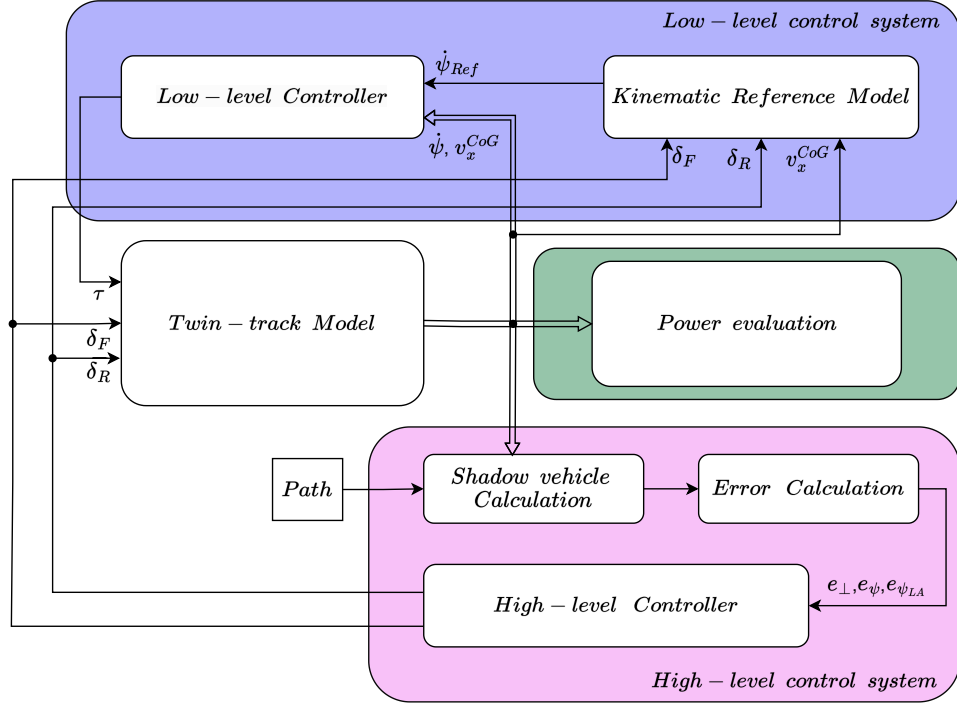

Figure 4.1: Framework Architecture

- Twin-track Model block includes implemented equations for twin-track model dynamics with used Tire models. The input of this block is the torque from the low-level controller and δ_f and δ_r, which are the steering angles of the front and rear wheels. The output of the block is a vector, which contains all needed state and output variables needed for control, computations, or visualization.

- Kinematic Reference Model block contains implemented equations of kinematic model. This block's input is the steering angles δ_f and δ_r and reference velocity taken from the Twin-track model. The output of this block is a vector, which contains state and output variables needed for the controller as a reference signal.

- Power Computation block contains all computations and visualizations related to power evaluation. Inputs of this block are variables from the twin-track model needed for the computation of powers. More is explained in the chapter 7.

- High-level control contains a cascade of controllers, which allow for the path-tracking task. Inputs of this block are computed errors and yaw of the vehicle. The output of this block is the steering angles δ_f and δ_r.

- Low-level control consists of a cascade of controllers and other blocks, which are traction control and asymmetric torque distribution. The input of this block is yaw rates of the twin-track model as the actual vehicle and of the kinematic model as a reference vehicle, longitudinal velocities of both of those models, and angular velocities of the twin-track model, which are further used as reference signals.

- In the Reference Generator block, the position of the shadow vehicle is being computed, which is also the output of this block.

- Error Calculations block contains calculations of cross-track errors and heading errors, which are also the outputs of this block.

4.3 Path Generation

The reference path is created using Matlab's Driving Scenario Designer application. This application, with its graphical user interface, provides a tool and visualisation to create a path by inserting points through which the path is to pass (See Fig. 4.2). These points are stored in a matrix of size $2 \times N$, where N is the number of points inserted. This matrix is stored in a *.mat* file and used to generate more points. The points (x_i, y_i) are
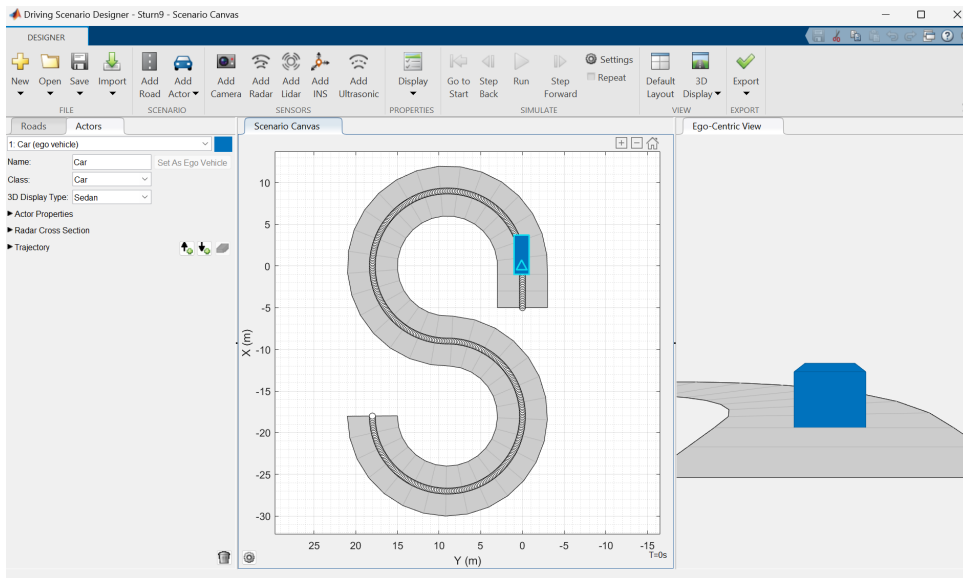

Figure 4.2: Screenshot of S-turn in Driving Scenario Designer

interpolated. If the path is a straight line, a perpendicular curve, a ramp,

29

or any other path consisting only of straight lines, the linear interpolation is used to make the path more defined. If the path consists of arcs, such as an S or U curve, quadratic interpolation is used. For circular or ellipsoidal paths, the path is generated as a circle or ellipse with a given radius and center. The interpolation should ensure the path's smoothness and increase the points' density. The order of the points is not parameterized by time, as it is a path and not a trajectory. However, the order of the points is the same as the order in which the points should be passed.

The reference friction coefficients μ_R and μ_L and the heading are also calculated. Different values of μ_R and μ_L can be used to demonstrate μ-split or μ-jump scenarios. The Matlab function to generate the path was taken from [Mac23] and extended by implementing the friction coefficients μ_R and μ_L. The points A, B and C in the Fig. 4.3 illustrate possible scenarios of μ-jump and μ-split. At first, all wheels are on the same surface with $\mu = 0.85$, corresponding to the asphalt or concrete friction coefficient. Next at point A, the μ on the right side of the road changes to $\mu = 0.2$, corresponding to ice or compacted snow. This situation is called μ-split. Next, the μ-split situation encounters the vehicle at point B, where the icy surface changes back to the road. Till point C, both sides have the same friction coefficient. At point C, both sides of the road change to icy surfaces again. This situation is referred to as μ-jump.
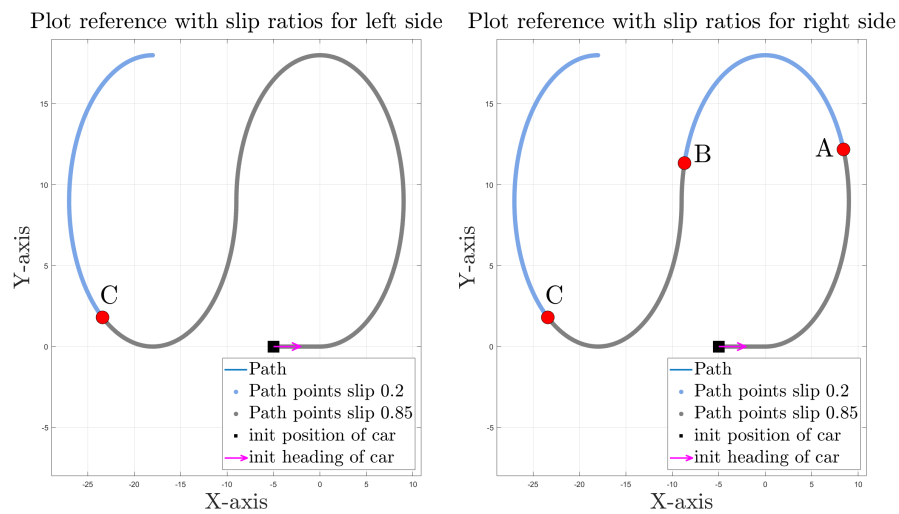

Figure 4.3: Interpolation of the same path as in 4.2 showing different values μ_L and μ_R for different parts of the path

Chapter 5

Low-level Control

In this chapter, the low-level control system is described. The low-level control consists of traction control/λ-control and asymmetric torque distribution. In the context of this thesis, this system is called torque vectoring, which is not an entirely accurate title or, more appropriately, a low-level control system.

Torque vectoring aims to change the vehicle dynamics in such a way that it improves the stability of the vehicle, especially under challenging conditions, and makes the vehicle more comfortable for the driver by improving the vehicle's maneuverability to reduce the driver's steering effort - eliminating understeering and oversteering. As mentioned in section 2.4, TV controls the distribution and transfer of engine torque to all driven wheels, allowing variable torque at each wheel. The controller designs for the TV system discussed in this chapter are presented as fundamental research in this area of vehicle dynamics. Along with a summary of the issues, this work provides a description of vehicle dynamics controllers.

5.1 Longitudinal Controller architecture

In this section, the architecture of the Torque Vectoring system is described. The controlling system is composed of a kinematic model and multiple controllers. First, the kinematic model, as already shown in Fig. 4.1, generates the reference yaw-rate $\dot{\psi}_{Ref}^{CoG}$ for the yaw-rate controller. The Yaw-rate and Velocity controllers operate parallel to generate references for the Slip ratio distribution block. The mapping block that maps slip ratio λ to the wheel angular speed ω and finally, the wheel angular speed controllers follow. The entire cascade structure is shown in Figure 5.1. It is a hierarchical architecture with three feedback loops and velocity, yaw-rate, and wheel angular speed controllers.
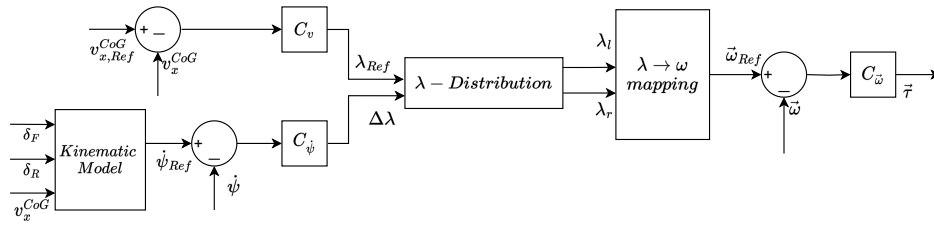
31

Figure 5.1: The architecture of the low-level controller

5.2 Yaw-rate controller

The goal of this controller is to minimize the deviation between the reference yaw-rate $\dot\psi_{Ref}$ given by the kinematic model and $\dot\psi$ of the vehicle. The controller's output is a slip ratio distribution $\Delta\lambda_{Ref}$ between the right and left wheels. The PI controller was used and designed at the working point velocity of 5 m/s. It was designed not to overshoot and, if so, less than 20% since, for the energy evaluation, overshooting is not efficient.

5.3 Velocity controller

The goal of this controller is to minimize the difference between the velocity of the vehicle v^{CoG} and the reference velocity v_{Ref}^{CoG}. The controller was designed as a PI regulator. The performance of this controller is influenced and restricted by the performance of the angular speed controller. Since the goal of this thesis was to focus on the energetic point of view, again, the regulator was designed to be less aggressive and to have a maximal overshoot of 20%. The step response from velocity $v_{Ref}^{CoG} = 5m/s$ to $v_{Ref}^{CoG} = 6m/s$ is shown in Fig. 5.2.
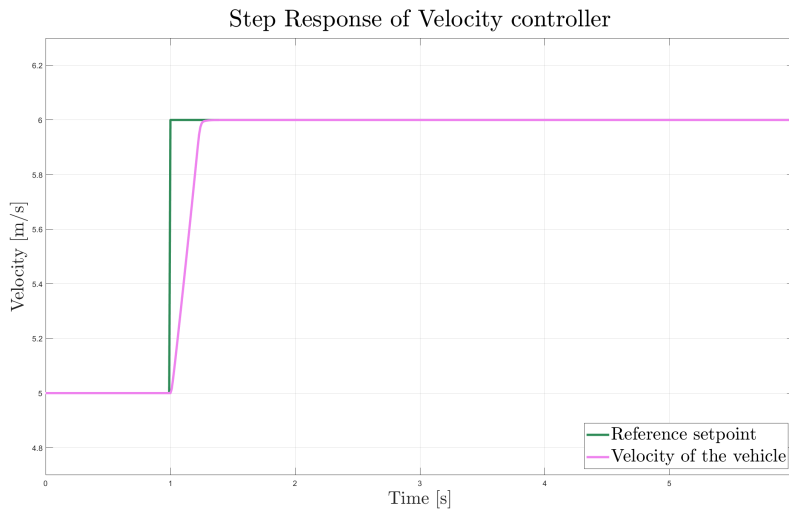
Figure 5.2: The step response of velocity controller

5.4 Slip ratio distribution

The actions of both previous controllers are used as a reference for the final slip ratio distribution between the right and left wheels. The distribution is illustrated below in Fig. 5.3 and given by Eq. 5.2.

$$\lambda_L = \lambda_{Ref} - \Delta\lambda \quad \text{,where } \lambda_L \in [-1, 1] \tag{5.1}$$

$$\lambda_R = \lambda_{Ref} + \Delta\lambda \quad \text{,where } \lambda_L \in [-1, 1] \tag{5.2}$$

Figure 5.3: The architecture of the slip ratio distribution block

33

■ 5.5 λ to ω mapping
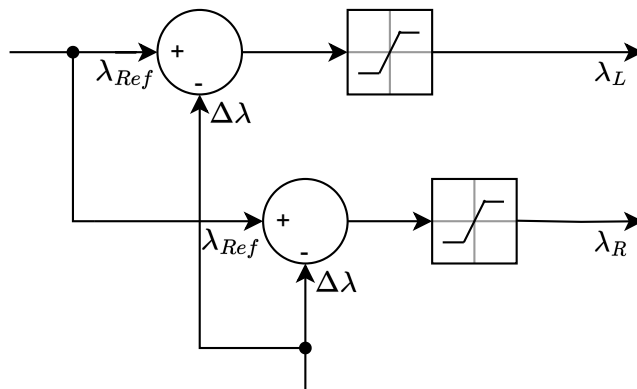
The computation of the angular speed of i-th wheel ω^i as a function of velocity v_x^i and slip ratio λ is done by using the equation 3.17 already mentioned earlier. There are four possible cases of the computation since the slip ration function is non-linear.

$$\omega^{w_i} = \begin{cases} \dfrac{v_x^i}{(1-\lambda) \cdot r} & \lambda \geq 0 \wedge v_x^{w_i} \geq 0, \\[3mm] \dfrac{v_x^{w_i} \cdot (1-\lambda)}{r} & \lambda \geq 0 \wedge v_x^{w_i} \leq 0, \\[3mm] \dfrac{v_x^{w_i} \cdot (1+\lambda)}{r} & \lambda \leq 0 \wedge v_x^{w_i} \geq 0, \\[3mm] \dfrac{v_x^{w_i}}{(1+\lambda) \cdot r} & \lambda \leq 0 \wedge v_x^{w_i} \leq 0 \end{cases} \tag{5.3}$$

■ 5.6 Wheel angular speed controller

The goal of this controller is to minimize the deviation between the reference angular speed ω^{w_i} and $\omega_{Ref}^{w_i}$ given by the previously mentioned controllers and mapping function. The controller's control actions are torques on all four wheels. The PI controller was used and designed at step response to $v_{Ref}^{CoG} = 5m/s$ to $v_{Ref}^{CoG} = 6m/s$, which is $\omega_{Ref}^{w_i} = 33.3rad/s$ to $\omega_{Ref}^{w_i} = 40rad/s$. It was designed not to overshoot and, if so, less than 20% since, for the energy evaluation, overshooting is not efficient. The step response is shown in Fig. 5.4. The difference between the angular wheel speed of front and rear wheels is due to the vehicle's parameters, such as the center of gravity.
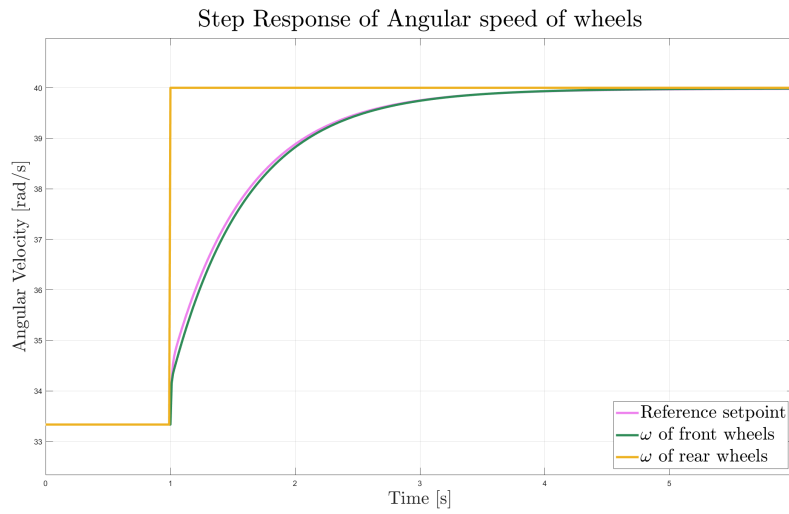
Figure 5.4: The step response of angular speed ω on front and rear wheels with the designed ω controller

▉ **5.7 Simulations**

The implementation of a low-level control system was tested on the circle maneuver at constant velocity $v = 5m/s$, and the torques on all four wheels were compared to each other. Fig. 5.5 shows the run for the architecture with both low-level and high-level control systems. The deficiency of high-level architecture gives the oscillations. The Fig. 5.6 shows the result for the architecture that uses only the low-level control system. Lastly, Fig. 5.7 shows the result for an architecture without control systems. The torque for this architecture is obtained by setting the $\Delta\lambda$ to zero; this way, there is no asymmetrical distribution between the right and the left side.

Torque on all wheels for circle maneuver at speed 5 m/s with usage of LLCS and HLCS
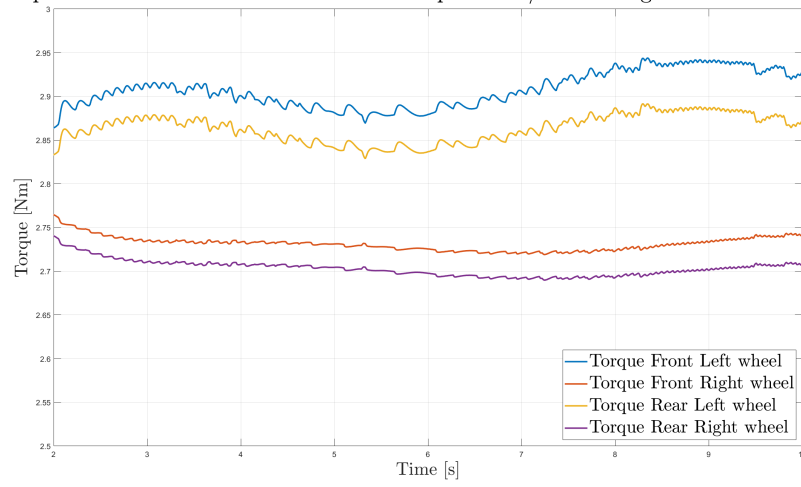
Figure 5.5: Torques on wheels for an architecture with both LLCS and HLCS

Torque on all wheels for circle maneuver at speed 5 m/s with usage of only LLCS
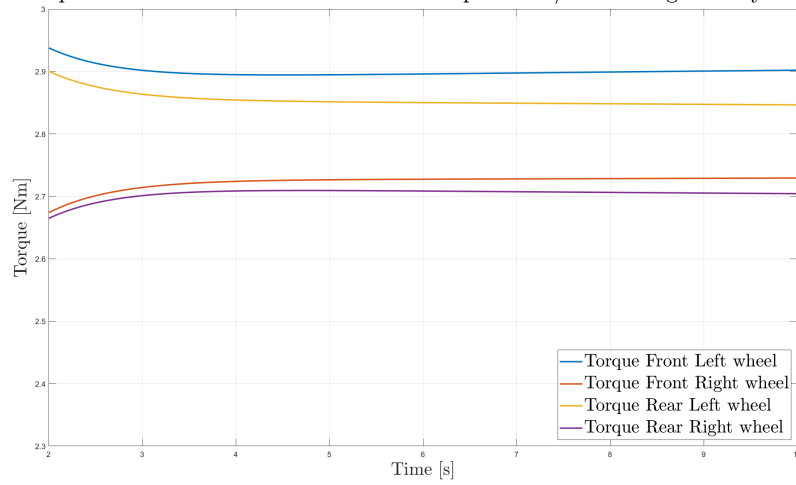
Figure 5.6: Torques on wheels for architecture with only LLCS

Torque of all wheels for circle maneuver at speed 5 m/s without any CS

Figure 5.7: Torques on wheels for an architecture without any CS

The asymmetrical distribution can be well seen in the figures 5.5 and 5.6. In the figure 5.7, it is clear that there is not any asymmetrical distribution between the right and left sides. The influence of the high-level control system is visible by comparison of the 5.5 and 5.6.

Chapter **6**

High-level Control

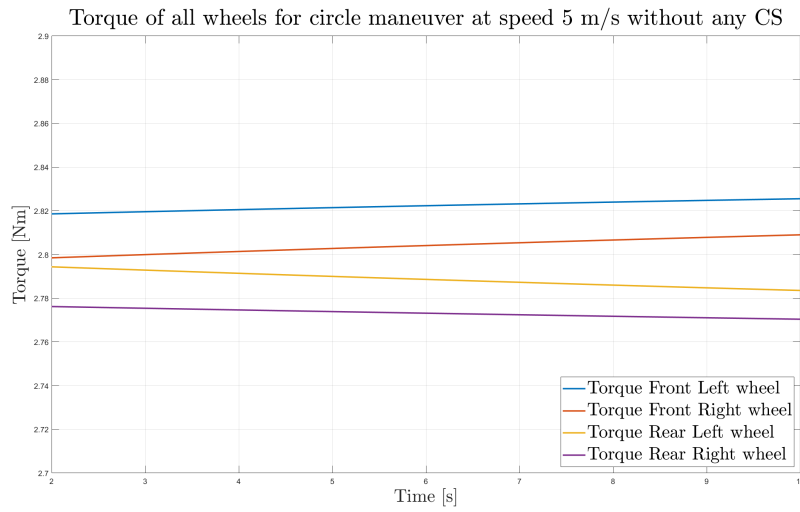The high-level controller aims to regulate the lateral direction to follow a reference path, as stated in section 2.2. In Robotics and Automation, the term *path* typically refers to a series of positions between an initial and final point without any time data. In contrast, a *trajectory* is a path that includes information about time. A reference path can be assigned a reference velocity or acceleration instead of being directly time-parameterized. However, this is not the case in this thesis. Measurable indicators must be defined for the lateral dynamics controllers to navigate the vehicle to follow the desired path.

6.1   Errors calculation

In this thesis, the indicators are cross-track error and heading error. Both of those broadly used to evaluate driving performance are described as the positional and the orientational error with respect to the reference path. The computation of those errors is further explained in sections below.

6.1.1   Cross-track Error

The cross-track error is a signed lateral deviation from the desired path. It directly indicates the vehicle's position with respect to the reference path. The sign of the error indicated if the vehicle is on the right side or left side next to to the path. For better understanding of the computation illustrations were provided (See Fig. 6.1a and 6.1b).

First the position of the shadow vehicle is calculated, meaning the point $\mathbf{W_1}$ with the minimal Euclidean distance is found. Then the next two

following points and two previous points from the reference path are taken and interpolated with spline. The interpolation temporarily increases the density of points. Next thank to the increased density of the points the closest point $\mathbf{W_2}$ on the spline is found as an orthogonal projection of the vehicle's position. Then the vector $\mathbf{y}$ is estimated as a tangent vector to the reference path at the point $\mathbf{W_2}$. The cross-track error is then computed as a length of vector $\mathbf{y}'$ (See Eq. 6.1.1).
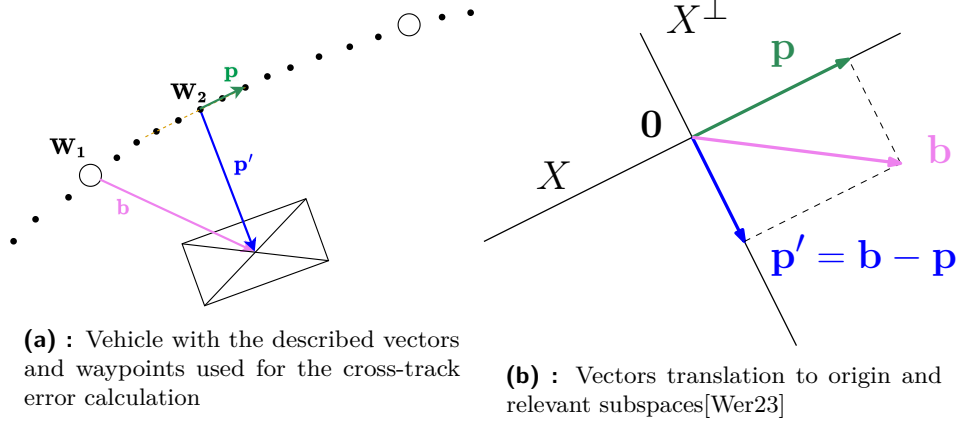

(a) : Vehicle with the described vectors and waypoints used for the cross-track error calculation

(b) : Vectors translation to origin and relevant subspaces[Wer23]

Figure 6.1:

$$e_\perp = ||\mathbf{p}'|| = \frac{\mathbf{p}^T}{||\mathbf{p}||}\mathbf{b}$$

■ 6.1.2 Heading Error

The heading error is the angular deviation between the vehicle's orientation and the desired direction needed to keep the vehicle aligned with the reference path in other words it is the deviation between the vehicle's yaw angle and the reference yaw angle. The heading ψ_{ref} is found using function *atan2* with its range $[-\pi, \pi]$. In the architecture of the high-level controller two heading errors are used. First the heading error e_ψ, which is the current heading error at the position of the vehicle (See. Eq. 6.1). Secondly the $e_{\psi_{LA}}$ is used, which is the heading error at the look-ahead position of the vehicle (See. Eq. 6.2). The calculation of heading error is shown in Fig. 6.2.

$$e_\psi = \psi_{ref} - \psi \tag{6.1}$$

$$e_{\psi_{LA}} = \psi_{ref,LA} - \psi \tag{6.2}$$
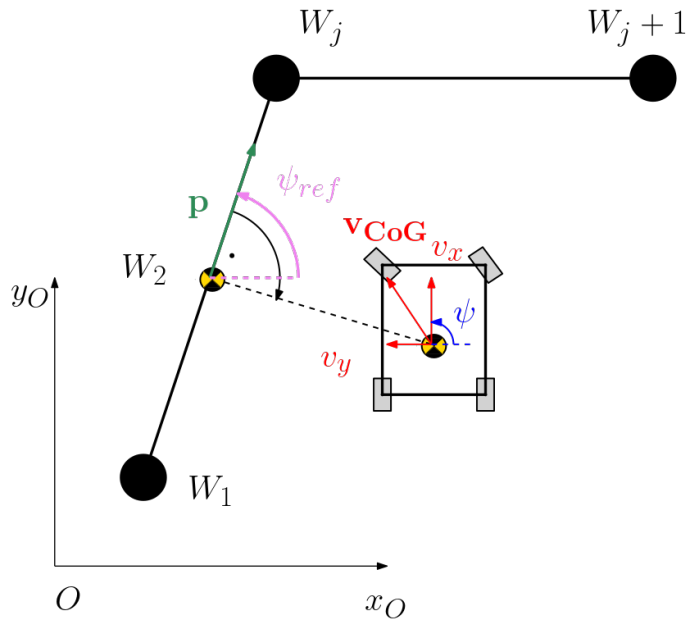
Figure 6.2: Graphical illustration for calculation of heading error

▌ 6.2   Lateral Controller architecture

The controller architecture is described in this section. The controller consists of two controllers, which are yaw controller and cross-track error controller. The structure is shown in the Fig.6.3.

Figure 6.3: The architecture of the high-level controller

▌ 6.3   Yaw Controller

The Yaw Controller is designed to minimize heading error and has been specifically engineered to prevent overshooting by more than 20%. Its input comprises the heading error, denoted as $\psi_{\text{ref}} - \psi$, and the control action of

41

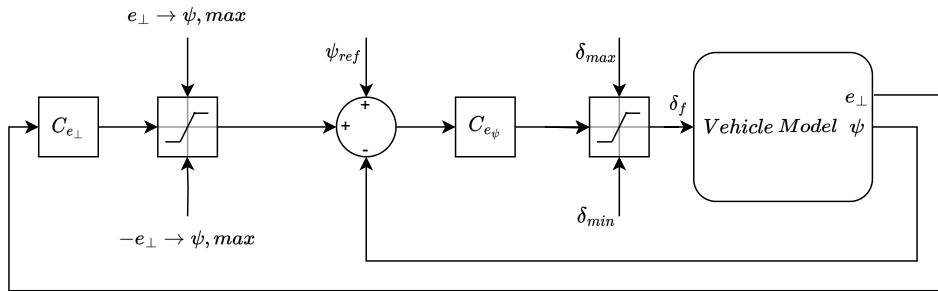the cross-track controller (refer to Fig. 6.3). The controller is configured as a PI regulator, operating at a constant velocity of the vehicle, $v^{\text{CoG}} = 5, \text{m/s}$. The primary objective is to generate a control action, denoted as ΔF. The controller's performance was evaluated through testing across various scenarios, including S-shaped turns, straight lines, and circles, at different velocities within the range $5 - 8 m/s$

◼ 6.4 Cross-Track Controller

Minimizing the cross-track error is the objective of the cross-track controller. The controller was designed as PI regulator, the regulator was designed at constant velocity $v^{\text{CoG}} = 5, \text{m/s}$. Its performance was evaluated by testing in a variety of scenarios, including S-shaped turns, straight lines, and circles, at various velocities within the range $5 - 8 m/s$.

Chapter 7

Power Evaluation

7.1 Power Calculations

In this section, the power efficiency evaluation, which is the main objective of this thesis, is presented. Power is the chosen physical quantity to describe the motion's energetic side. *Power* is defined as "the time rate of doing work or delivering energy, expressible as the amount of work done W, or energy transferred, divided by the time interval t" [Briar], with its SI Unit Watt. This definition can be written as an equation 7.1, where P denotes the power and W work.

$$P = \frac{dW}{dt} \tag{7.1}$$

In the context of EVs, power is generated by the powertrain, which includes the electric motor, transmission (if applicable), and other relevant components. This power is transferred to the wheels as torque (See Eq. 7.3). For simplification, the power consumption of AC, lights, etc., is neglected, as only the model of the EV is used in this thesis. A further assumption is, as already mentioned in section 3.7, that the powertrain was for the purposes not implemented. So, the time constant, stiffness of the powertrain/drivetrains, and damping effects are not being considered here. The equations used in this thesis for the computation of power are derived from the equations 7.2 and 7.3. However, those equations are general equations for mechanical power expressed as a product of force $\mathbf{F}$ and $\mathbf{v}$ 7.2 and mechanical power expressed as a product of τ and angular velocity ω 7.3.

$$P = \frac{d}{dt}(\mathbf{F} \cdot \mathbf{r}) = \mathbf{F} \cdot \frac{d\mathbf{r}}{dt} = \mathbf{F} \cdot \mathbf{v} \tag{7.2}$$

$$P = \frac{dW}{dt} = \boldsymbol{\tau} \cdot \boldsymbol{\omega} \tag{7.3}$$

■ 7.1.1 Power Calculations - vehicle's level

The following equations were used to calculate power on the vehicle's level. First, the equations 7.4 and 7.5 express the power of the vehicle.

$$P_\psi = \tau_{CoG} \cdot \dot{\psi} \tag{7.4}$$

$$\begin{aligned} P_\psi = \dot{\psi} \left(\frac{d}{2}(F_x^{FR} + F_x^{RR} - F_x^{FL} - F_x^{RL}) \right. \\ \left. + (F_y^{FL} + F_y^{FR}) \cdot l_f - (F_y^{RL} + F_y^{RR}) \cdot l_r \right) \end{aligned} \tag{7.5}$$

$$\begin{bmatrix} P_x \\ P_y \\ P_\psi \end{bmatrix} = \begin{bmatrix} F_x^V \\ F_y^V \\ T_\psi^V \end{bmatrix} \cdot \begin{bmatrix} v_x^V \\ v_y^V \\ \omega_\psi^V \end{bmatrix}^T \tag{7.6}$$

$$P = P_x + P_y + P_\psi \tag{7.7}$$

■ 7.1.2 Power Calculations - wheel's level

For power efficiency evaluation on the wheel's level, the equation for power expressed as a function of force and velocity is useful since it directly gives the power losses in both longitudinal and lateral directions due to the acting of longitudinal and lateral force, respectively. This is shown in Eq.7.2 and 7.9. In Eq. 7.8 and 7.9, the power P_ω^i given by torque transferred from the engine on the vehicle is stated.

$$P_{w_i,\omega} = \tau^{w_i} \cdot \omega^{w_i} \tag{7.8}$$

$$\begin{bmatrix} P_{w_i,x} \\ P_{w_i,y} \\ P_{w_i,\omega} \end{bmatrix} = \begin{bmatrix} F_x^{w_i} \\ F_y^{w_i} \\ T^{w_i} \end{bmatrix} \cdot \begin{bmatrix} v_x^{w_i} \\ v_y^{w_i} \\ \omega^{w_i} \end{bmatrix}^T \tag{7.9}$$

- ■ $P_{w_i,\omega}$ denotes mechanical power delivered to the wheel, converted into forward motion (or braking).

- ■ τ^{w_i} is the transferred torque on the i-th wheel.

- ■ ω^{w_i} angular speed of the i-th wheel.

- ■ $P_{w_i,x}$, $P_{w_i,y}$, $P_{w_i,\omega}$ are components of power of the i-th wheel.

- ■ $F_x^{w_i}$, $F_y^{w_i}$ are components of forces acting on the i-th wheel.

- ■ T^{w_i} is the transferred torque on the i-th wheel.

- ■ $v_x^{w_i}$, $v_y^{w_i}$, ω^{w_i} are components of velocity and angular velocity of the i-th wheel.

■ 7.2 Simulation

The power is evaluated in multiple scenarios. First, there are two different shapes of reference path - a circle maneuver and an S-shaped turn. Since both reference paths can have various radii, the power is compared on circles and S-turns of different radii. Another factor that can have an impact on power usage is the velocity; that is why some of the scenarios are tested for different velocities. Three architectures are compared - a vehicle that uses both low-level and high-level control systems (further in graphs referred to as LLCS and HLCS). The following vehicle uses only the low-level control system and has manually set the steering angles on the front wheels. Lastly, as a baseline, a vehicle that does not use any control system, meaning the steering angles on front wheels are set manually, and the same steady state value of torque is transferred to all wheels.

In the interest of conciseness and to avoid overwhelming the reader with excessive data, I have decided not to include all graphs for every power of every wheel and CoG that can be generated. This decision is motivated by a desire to maintain clarity and prevent over-stimulation, allowing the focus to remain on the most important and insightful stuff.

■ 7.3 Circle maneuver

Here, the architecture was tested on a circle scenario with a radius of 10m. The simulations were conducted for two different velocities for constant friction coefficients $\mu = 0.9$, which corresponds to the asphalt or concrete surface of the road.

The figures 7.1 and 7.2 compare the total power at the vehicle level. From those pictures it seems that the power usage of the vehicle without any CS is the lowest. However, the power usage of the engine is not covered here. This power describes only the power generated by the forces and yaw moment acting on the vehicle at the center of gravity. Another thing to observe here is the difference in the amplitude for both of the velocities. The Fig. 7.1 shows the power for vehicle driving with velocity $v = 5m/s$, which is $18km/h$. The Fig. 7.2 shows the power for vehicle driving with velocity $v = 7m/s$, which is $25.2km/h$.
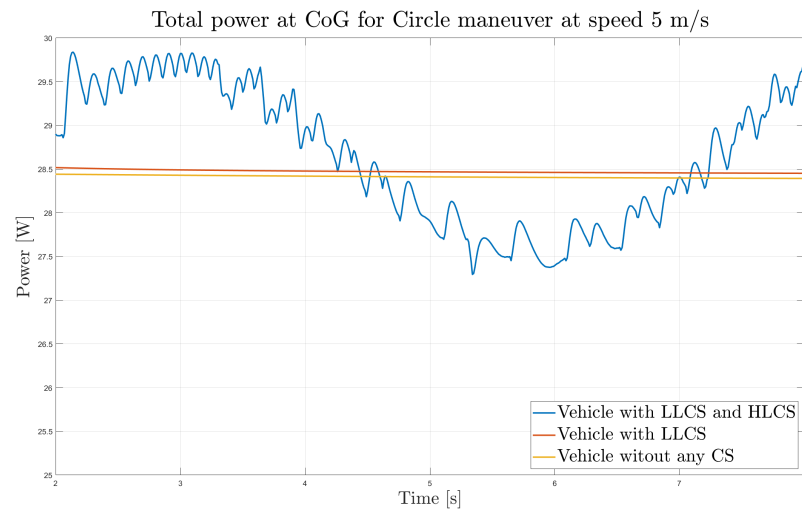
Figure 7.1: Total power of a vehicle for circle maneuver at speed 5m/s
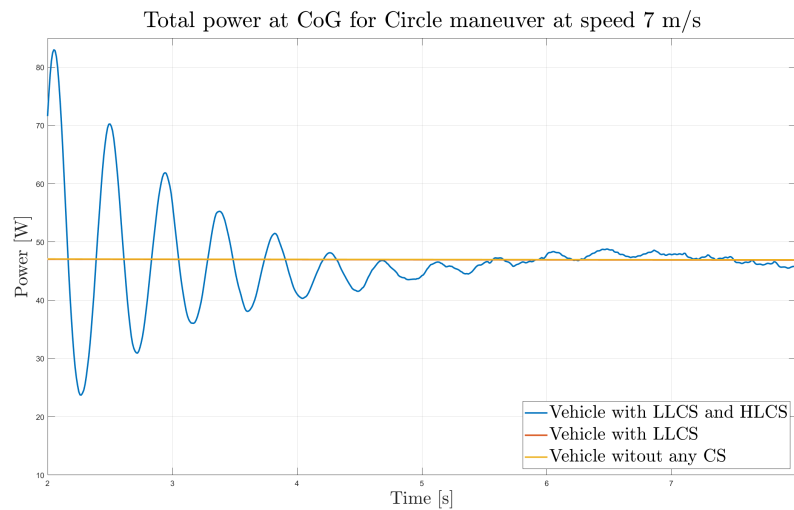

Figure 7.2: Total power of a vehicle for circle maneuver at speed 7m/s

The figures 7.3 and 7.4 both illustrate the power given by the longitudinal force and velocity of front wheels again for velocities $v = 5m/s$ and $v = 7m/s$. Again, the power generated by the longitudinal force and velocity are higher for the higher velocity. The fascinating insight here is that as all three described architectures are displayed, the difference between the forces of the front left wheel and front right wheel is the highest for the vehicle without any CS. For the architectures using LLCS, the difference is significantly lower. The influence of the deficiency of the high-level control system is visible; however, the influence of the low-level control system is not shadowed.
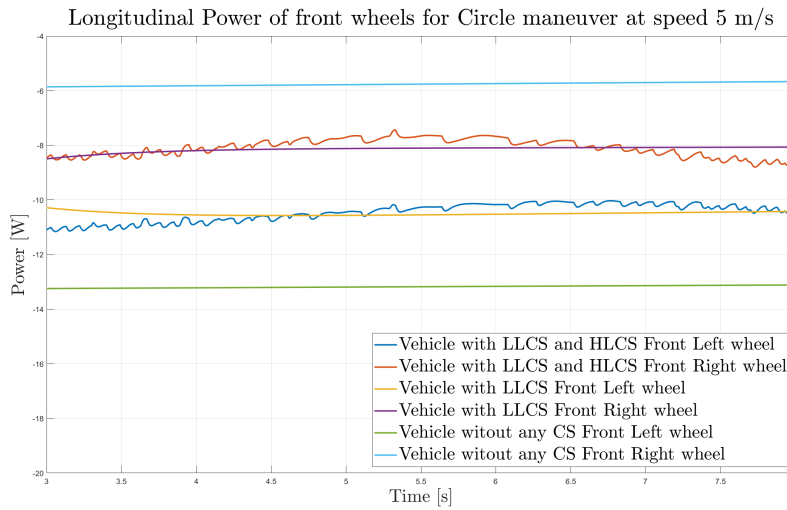
Longitudinal Power of front wheels for Circle maneuver at speed 5 m/s

Figure 7.3: Power given by the longitudinal force and velocity of front wheels at speed 5m/s

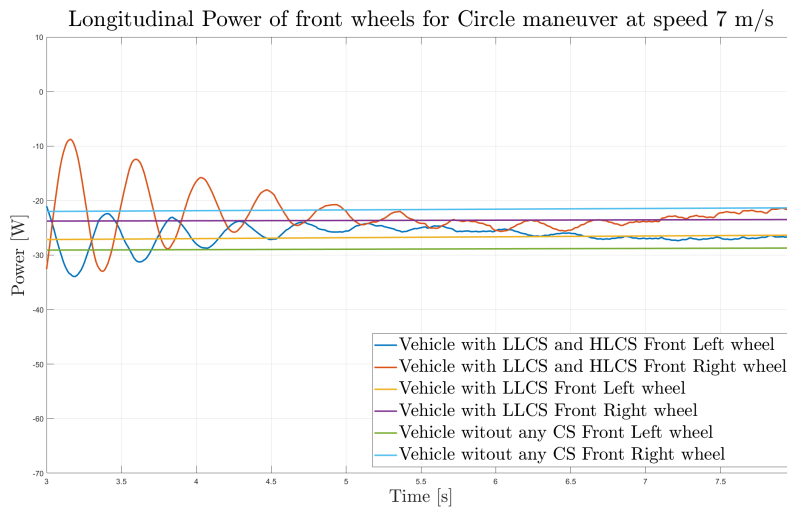Longitudinal Power of front wheels for Circle maneuver at speed 7 m/s

Figure 7.4: Power given by the longitudinal force and velocity of front wheels at speed 7m/s

The figures 7.5 and 7.6 provide the graphs of power transferred from the engine to the front wheels at velocities $v = 5m/s$ and $v = 7m/s$. Again, comparing the amplitudes for higher and lower speeds provides interesting insight. However, the difference between the right and left wheels for the same architecture is more interesting. The difference for the vehicle without any CS is the lowest since there is no asymmetrical torque distribution between the right and left sides. Despite the oscillations of the system with HLCS, it is visible that the value around which the system is oscillating is the same as that of the vehicle that uses only LLCS.

47

Power transferred from engine to front wheels for Circle maneuver at speed 5 m/s
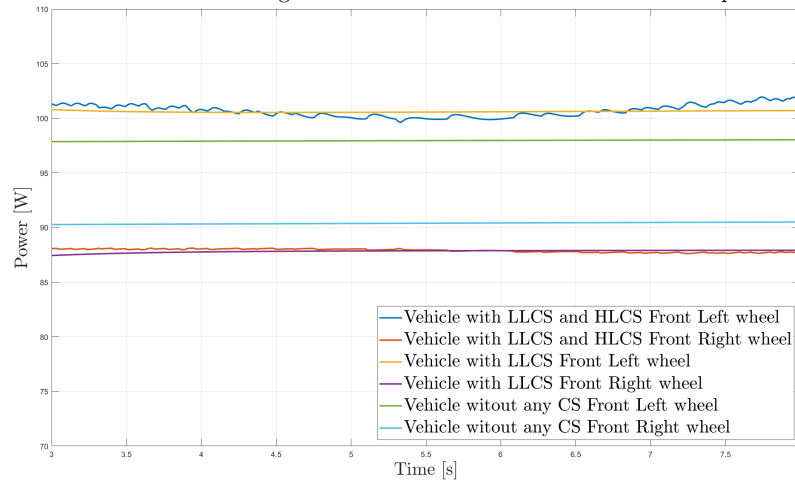

Figure 7.5: Power transferred from the engine to front wheels at speed 5m/s

Power transferred from engine to front wheels for Circle maneuver at speed 7 m/s
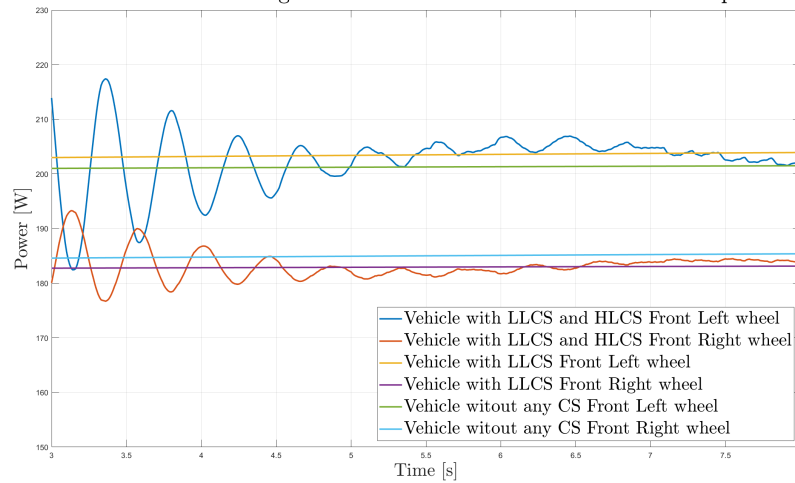
Figure 7.6: Power transferred from the engine to front wheels at speed 7m/s

7.4 S-turn maneuver

This section presents the tests of the architecture on an S-shaped turn scenario. The simulation was conducted for two different velocities for constant friction coefficients $\mu = 0.9$, corresponding to the asphalt or concrete surface of the road. The tests were run on two S-shaped paths with different radii.

First, the figures 7.7 and 7.8 show the total power of a vehicle for an S-turn maneuver with radius r = 12m for two different velocities $v = 5m/s$ and

$v = 7m/s$. Despite the oscillations, the vehicle's steady-state power value using both HLCS and LLCS is lower than that of vehicles using only LLCS or no CS. This can be see in Fig. 7.7 at time interval $[2, 11]$ and $[13.5, 16]$. The same thing can be observed in the figure 7.8 at time interval $[4, 6]$ and $[13.5, 16]$. It is also visible that here, the amplitude of the oscillations depends on the velocity.
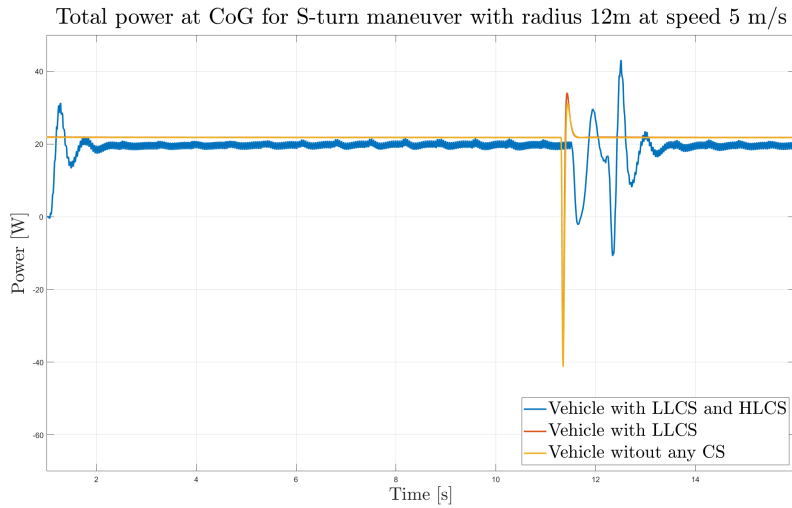

Figure 7.7: Total power of a vehicle for S-turn maneuver with radius $r = 12m$ at speed 5m/s
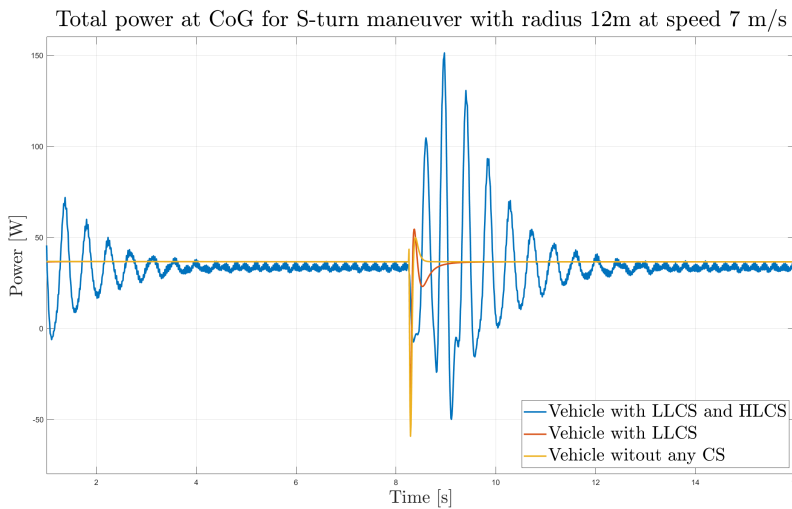
Figure 7.8: Total power of a vehicle for S-turn maneuver with radius $r = 12m$ at speed 7m/s

Figures 7.9, 7.10, 7.11, and 7.12 all display the power given by the longitudinal force and velocity of all four wheels. The power dependency on

the radius of the turn and the dependency on the velocity can be observed. The smaller the radius, the higher the power of the wheels. All the figures correspond to the architecture using only LLCS.

Figure 7.9: Power given by the longitudinal force and velocity of all four wheels at speed 5m/s for S-turn maneuver with radius $r = 12m$

Figure 7.10: Power given by the longitudinal force and velocity of all four wheels at speed 7m/s for S-turn maneuver with radius $r = 12m$

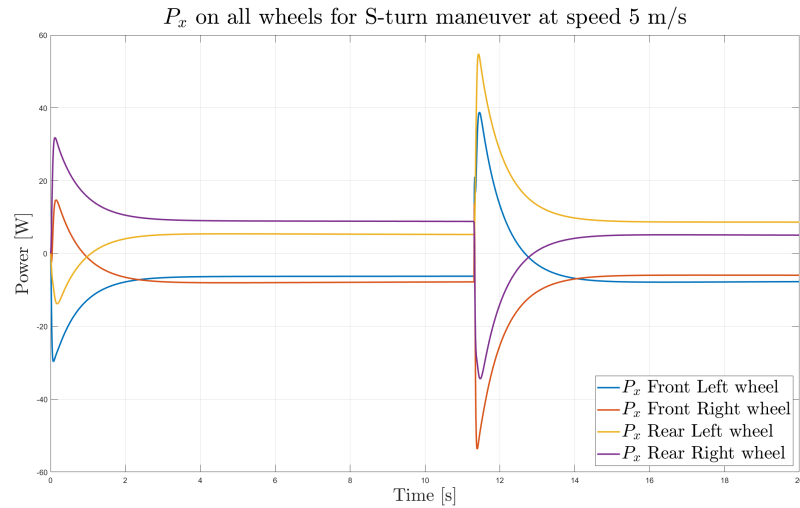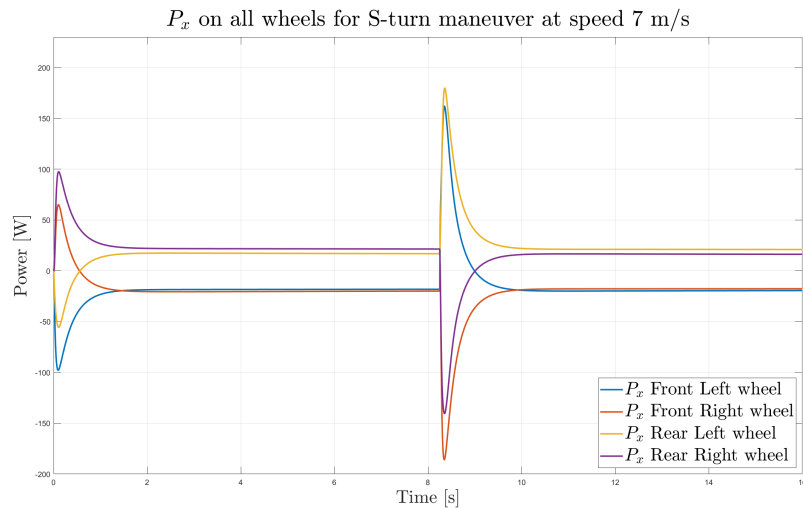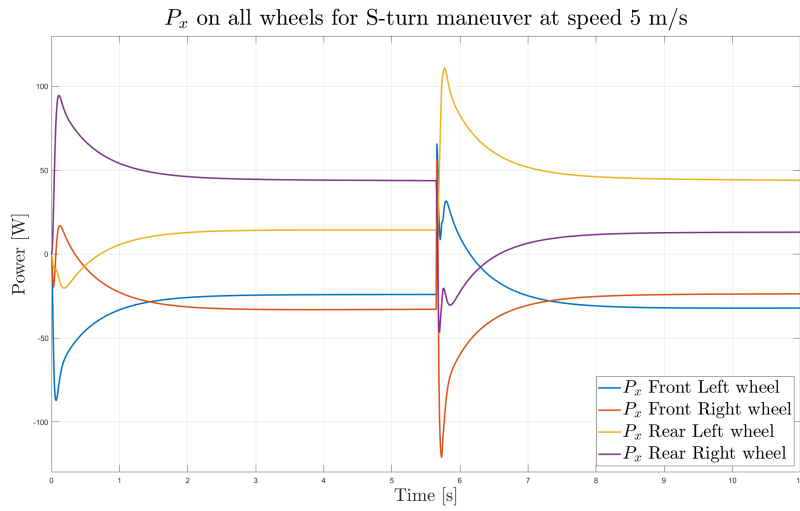**Figure 7.11:** Power given by the longitudinal force and velocity of all four wheels at speed 5m/s for S-turn maneuver with radius $r = 6m$
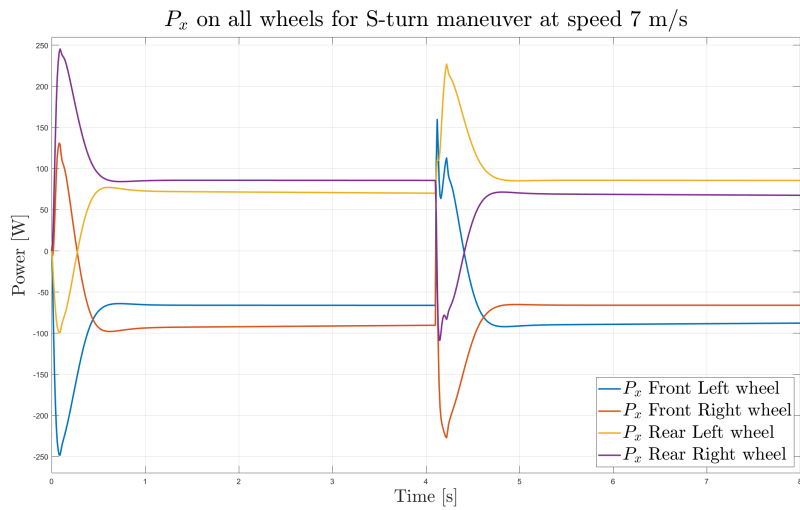

Figure 7.12: Power given by the longitudinal force and velocity of all four wheels at speed 7m/s for S-turn maneuver with radius $r = 6m$

Chapter 8

Conclusion

8.1   Results Summary

The objective of this thesis was to develop a suitable algorithm or methodology for evaluating the energy efficiency of over-actuated vehicles, focusing on vehicle dynamic control and high-level path tracking algorithms.

For this thesis, a twin-track model, a reference kinematic model, a low-level control system, and a high-level control system were designed. The reason for choosing this architecture was the following: a path-tracking algorithm was needed to ensure the repeatability of the maneuvers. A kinematic model was chosen as a reference model since its sideslip angles are considered equal to zero, and such a model can lead to minimizing the driving resistances. Next, the traction control and asymmetric slip ratio distribution were designed with the kinematic model as a reference. The mathematical models are discussed in the first part of the thesis. The design of the high-level and low-level control systems was discussed in the second part of this work. In the last part, this architecture was tested on several driving scenarios. The power usage of the vehicle using both control systems was compared to the power usage of the architecture using only the low-level control system and to the baseline architecture using no control system. The result showed a significant improvement while using the low-level control system. However, the vehicle's power usage using both control systems was higher than expected. This is because of multiple reasons, one needing more precise tuning of the HLCS. The performance can be improved. This deficiency led to higher power usage than expected. Nevertheless, for S-turn maneuver at both velocities $v = 5$m/s and $v = 7$m/s for particular time intervals, it can be observed that the power of the motion of the vehicle using both CS is lower than the usage of the vehicle without any CS and also lower than the usage of a vehicle using LLCS. On the other hand, the influence of the low-level control system on the vehicle

is considerable. Not only does the asymmetric distribution provide higher stability of the vehicle, but also the distribution of the torques, and so the distribution of the power needed to be transferred from the engine to each wheel is for scenarios such as driving in turns and curves distributed more efficiently.

◼ 8.2 Future Work

◼ Improvement of high-level control system

As already mentioned, this thesis's deficiency is the need for more focus on precise tuning of the controllers. This can still be developed to improve the performance and minimize the power usage and performance on circles or S-shaped turns with smaller radii.

◼ 8.2.1 Experiments on validation platform

This model is designed to be tested experimentally on a validation platform which is still under development. The comparison of simulations and physical experiments can provide interesting insights.

◼ 8.2.2 Quantification of power losses

Detailed evaluation of the efficiency and analysis of driving resistance of the vehicle and wheels for different driving scenarios and quantification of the isolatable or controllable factors such as aerodynamics, friction, and rolling resistance.

Appendix A

Bibliography

[Bor13]   A. Boretti, *Analysis of the regenerative braking efficiency of a latest electric vehicle*, Tech. Report 2013-01-2872, SAE Technical Paper, 2013, Accessed: 28.12.2023.

[Briar]   Encyclopedia Britannica, *Power*, Year, Accessed: Date.

[Cha93]   C. C. Chan, *An overview of electric vehicle technology*, Proc. IEEE **81** (1993), no. 9, 1202–1213.

[Cha02]   _____, *The state of the art of electric and hybrid vehicles*, Proc. IEEE **90** (2002), no. 2, 247–275.

[Cib19]   Vít Cibulka, *Mpc based control algorithms for vehicle control*, `http://hdl.handle.net/10467/82396`, 05 2019, Accessed: 28.11.2023.

[DNSG14]   Leonardo De Novellis, Aldo Sorniotti, and Patrick Gruber, *Wheel torque distribution criteria for electric vehicles with torque-vectoring differentials*, IEEE Transactions on Vehicular Technology **63** (2014), no. 4, 1593–1602.

[DS14]   Roberto Bardini Dieter Schramm, Manfred Hiller, *Vehicle dynamics, modeling and simulation*, Springer, 2014.

[ELR08]   A. Emadi, Y. Lee, and K. Rajashekara, *Power electronics and motor drives in electric, hybrid electric and plug-in hybrid electric vehicles*, IEEE Trans. Ind. Electron. **55** (2008), no. 6, 2237–2245.

[FAR16]   Chiara Fiori, Kyoungho Ahn, and Hesham A. Rakha, *Power-based electric vehicle energy consumption model: Model development and validation*, Applied Energy **168** (2016), 257–268.

[FKF$^+$13]   Saber Fallah, Amir Khajepour, Baris Fidan, Shu-Kun Chen, and Bakhtiar Litkouhi, *Vehicle optimal torque vectoring using state-derivative feedback and linear matrix inequality*, IEEE Transactions on Vehicular Technology **62** (2013), no. 4, 1540–1552.

[Han23]   Tomáš Haniš, *Mathematical models*, Automotive Control Systems - B3M35RSA.

[Int11]   International Organization for Standardization, *Road vehicles - vehicle dynamics and road-holding ability - vocabulary*, Tech. Report ISO 8855, ISO, 2011.

[KM97]   H. Kahlen and G. Maggetto, *Electric and hybrid vehicles*, Proc. EPE Conf., vol. 1, September 1997, pp. 1030–1054.

[Mac23]   Jakub Macar, *Over-actuated vehicles path tracking algorithms*, `https://dspace.cvut.cz/handle/10467/109035`, 05 2023, Accessed: 25.11.2023, p. 8.

[MB16]   Rashid Mehmood and Umar Bhatti, *Coarse determination of attitude using a single gps receiver*, 04 2016.

[MERE99] J. M. Miller, A. Emadi, A. V. Rajarathnam, and M. Ehsani, *Current status and future trends in more electric car power systems*, Proc. IEEE Veh. Technol. Conf., May 1999, pp. 1380–1384.

[Mon18]   Martin Mondek, *Active torque vectoring systems for electric drive vehicles*, `http://hdl.handle.net/10467/73936`, 01 2018, Accessed: 30.11.2023.

[Mut12]   Nobuyoshi Mutoh, *Driving and braking torque distribution methods for front- and rear-wheel-independent drive-type electric vehicles on roads with low friction coefficient*, IEEE Transactions on Industrial Electronics **59** (2012), no. 10, 3919–3933.

[Pac05]   Hans B. Pacejka, *Tire and vehicle dynamics (second edition)*, second edition ed., Butterworth-Heinemann, Oxford, 2005.

[PLRG10] Damrongrit Piyabongkarn, Jae Young Lew, Rajesh Rajamani, and John A. Grogg, *Active driveline torque-management systems*, IEEE Control Systems **30** (2010), 86–102.

[Raj12]   Rajesh Rajaman, *Vehicle dynamics and contro (second edition)*, second edition ed., Springer, 2012.

[Tur19]   Petr Turnovec, *Vehicle slip ratio control system for torque vectoring functionality*, `https://dspace.cvut.cz/handle/10467/83062`, 05 2019, Accessed: 15.11.2023, p. 3.

[U.S23a]   U.S. Energy Information Administration, *The International Energy Outlook*, U.S. Energy Information Administration (2023), Accessed: 28.12.2023.

[U.S23b]   _____ , *The International Energy Outlook*, U.S. Energy Information Administration (2023), Accessed: 28.12.2023.

[VH23]   David Vošahlík and Tomáš Haniš, *Traction control alloca-tion employing vehicle motion feedback controller for four-wheel-independent-drive vehicle.*

[VS04]   Editor in Chief Cutler J. Cleveland Vaclav Smil, *Encyclopedia of energy, world history and energy*, vol. 6, Elsevier Science, 2004, Accessed via http://vaclavsmil.com/wp-content/uploads/docs/smil-article-2004world-history-energy.pdf.

[Wer23]   Tomáš Werner, *Optimalizace*, Accessed: 26.12.2023.

[YW12]   Xibo Yuan and Jiabin Wang, *Torque distribution strategy for a front- and rear-wheel-driven electric vehicle*, IEEE Transactions on Vehicular Technology **61** (2012), no. 8, 3365–3374.

[Šv23]   Jan Švancar, *Autonomous vehicle trajectory tracking algorithms*, 2023.